Neurotherapeutics (2023) 20:1405–1426
https://doi.org/10.1007/s13311-023-01420-1

ORIGINAL ARTICLE

Fecal Microbiota Transplantation from Aged Mice Render Recipient Mice Resistant to MPTP-Induced Nigrostriatal Degeneration Via a Neurogenesis-Dependent but Inflammation-Independent Manner

Chen-Meng Qiao[1] · Yu Zhou[1] · Wei Quan[1] · Xiao-Yu Ma[1] · Li-Ping Zhao[1] · Yun Shi[1] · Hui Hong[1] · Jian Wu[1] · Gu-Yu Niu[1] · Yu-Nuo Chen[1] · Shan Zhu[1] · Chun Cui[1] · Wei-Jiang Zhao[1] · Yan-Qin Shen[1]

Accepted: 26 July 2023 / Published online: 18 August 2023

Abstract

Accumulating data support a crucial role of gut microbiota in Parkinson's disease (PD). However, gut microbiota vary with age and, thus, will affect PD in an age-dependent, but unknown manner. We examined the effects of fecal microbiota transplantation (FMT) pretreatment, using fecal microbiota from young (7 weeks) or aged mice (23 months), on MPTP-induced PD model. Motor function, pathological changes, striatal neurotransmitters, neuroinflammation, gut inflammation and gut permeability were examined. Gut microbiota composition and metabolites, namely short-chain fatty acids (SCFAs), were analyzed. Neurogenesis was also evaluated by measuring the number of doublecortin-positive (DCX^+) neurons and Ki67-positive ($Ki67^+$) cells in the hippocampus. Expression of *Cd133* mRNA, a cellular stemness marker, in the hippocampus was also examined. Mice who received FMT from young mice showed MPTP-induced motor dysfunction, and reduction of striatal dopamine (DA), dopaminergic neurons and striatal tyrosine hydroxylase (TH) levels. Interestingly and unexpectedly, mice that received FMT from aged mice showed recovery of motor function and rescue of dopaminergic neurons and striatal 5-hydroxytryptamine (5-HT), as well as decreased DA metabolism after MPTP challenge. Further, they showed improved metabolic profiling and a decreased amount of fecal SCFAs. High-throughput sequencing revealed that FMT remarkably reshaped the gut microbiota of recipient mice. For instance, levels of genus *Akkermansia* and *Candidatus Saccharimonas* were elevated in fecal samples of recipient mice receiving aged microbiota (AM + MPTP mice) than YM + MPTP mice. Intriguingly, both young microbiota and aged microbiota had no effect on neuroinflammation, gut inflammation or gut permeability. Notably, AM + MPTP mice showed a marked increase in DCX^+ neurons, as well as $Ki67^+$ cells and *Cd133* expression in the hippocampal dentate gyrus (DG) compared to YM + MPTP mice. These results suggest that FMT from aged mice augments neurogenesis, improves motor function and restores dopaminergic neurons and neurotransmitters in PD model mice, possibly through increasing neurogenesis.

Keywords Fecal microbiota transplantation (FMT) · Aged microbiota · Parkinson's disease (PD) · Inflammation · Neurogenesis

Introduction

The gut microbiota, a significant microbiota in the host, not only affects intestinal physiology, but also modulates host immune and endocrine systems [1–4]. In last decade, a rapid growing body of studies have documented that the gut microbiota and their metabolites play important roles in central nervous system (CNS) development, including formation of the blood–brain barrier, neurogenesis and maturation of microglia [5–7], and shape the onset, severity and/or progression of a number of neurodegenerative disorders, for instance, Parkinson's disease (PD) [8–11].

PD is a disease with high incidence in the elderly and characterized by the loss of dopaminergic neurons and neurotransmitters. It is clinically characterized by motor symptoms (including bradykinesia, resting tremor, and rigidity) and non-motor symptoms (including dysphagia and gastrointestinal (GI) dysfunction, such as constipation and intestinal

Chen-Meng Qiao and Yu Zhou contributed equally.

✉ Yan-Qin Shen
shenyanqin@jiangnan.edu.cn

[1] Laboratory of Neurodegeneration and Neuroinjury, Wuxi School of Medicine, Jiangnan University, Wuxi, Jiangsu 214122, China

microflora dysbiosis). Notably, non-motor symptoms occur frequently in PD and may even precede motor symptoms [12, 13]. Accumulating evidence shows that alterations in gut microbiota composition and microbial metabolites are closely related to the pathogenesis and clinical phenotype of PD [14, 15]. For instance, Keshavarzian et al. found a decrease in the abundance of *Blautia*, *Coprococcus*, and *Roseburia* in PD after analyzing the microbiota of sigmoid mucosal biopsies and stool samples in PD patients [16]. Moreover, the abundance of *Enterobacteriaceae* is positively correlated with severity of postural instability and gait difficulty, suggesting that dysbiosis in the microbiome of PD patients is related to the motor phenotype [10]. As for laboratory studies, Torres and colleagues found a lower phylogenetic diversity of microbiomes associated with MPTP-treated mice compared to saline-treated mice [17]. Additionally, Sampson et al. revealed that alterations in gut microbial metabolic, short-chain fatty acids, was sufficient to promote αSyn-mediated neuroinflammation [8]. These studies reveal a strong correlation between gut microbiota and PD, further demonstrating that gut microbiota plays an important role in neurological regulation.

Aging is usually characterized by inflammation and gut dysbiosis. Aging-related chronic inflammation, is a cardinal feature and a risk factor for the development of age-associated pathologies such as stroke, Alzheimer's disease (AD), and PD. The pathophysiological implications of microbiota have expanded considerably in recent years. The transfer of aging microbiota to young germ-free mice promotes the inflammation in the small intestine of the germ-free mice and increases the abundance of TM7 and *Proteobacteria* [18]. Aged stroke mice receiving aged fecal transplant gavage have more behavioral impairment, and more brain and gut inflammation than those mice receiving young fecal transplant gavage [19], and young stroke mice receiving aged fecal transplant gavage show decreased performance on behavioral tests and increased mortality following MCAO [20], suggesting a negative role of microbiota from aged mice in neuroprotection. FMT of elderly donor mice triggered phenotypic changes in glia cells of the hippocampus fimbria but did not affect gut permeability or levels of systemic and brain cytokines [21]. Inconsistently, some studies imply that microbiota from older mice may be neuroprotective. Kundu et al. found that transferring microbiota from old mice into young germ-free mice confers increased neurogenesis in the hippocampus of the brain, suggesting that gut microbiota transplants from aged hosts can confer beneficial effects in responsive young recipients [6]. However, it is completely unknown how microbiota from aged donors influence the brain and gut in PD. Given the difference of gut microbiota between young and aged hosts, we propose that the extent, by which the microbiome affects the pathological features of PD, is dependent on the age of the host from which the microbiome is derived.

Here, we first give antibiotics by gavage to the recipient mice in order to deplete their gut microbiota. Then FMT, using fecal microbiota from young or aged donor mice (hereafter referred to as young or aged microbiota, respectively), was performed on the above recipient mice before MPTP modeling (PD mice) or saline injections (control mice). We found that FMT with aged microbiota could modify the MPTP-induced motor dysfunction, and rescue the loss of dopaminergic neurons, decrease the metabolism of striatal DA and elevate the striatal 5-hydroxytryptamine (5-HT) in PD mice. The impact of age-associated shifts of microbiota on PD mice was further confirmed by the observation that FMT using aged microbiota, prior to induction of PD, improved gut microbial dysbiosis and promoted neurogenesis of the hippocampus, as well as lowered fecal concentrations of SCFAs in PD mice. Unexpectedly, these changes occurred in the absence of an overt increase of both striatal and colonic levels of pro-inflammatory cytokines and intestinal permeability, indicating aged microbiota confers resistance to MPTP in a neurogenesis-dependent, inflammation-independent manner.

Materials and Methods

Animals and Experimental Groups

Young (7 weeks) and aged (23 months) male C57BL/6 J mice served as fecal microbiota donor mice, adult (8 weeks) male C57BL/6 J mice served as fecal microbiota recipient mice. Mice (Vital River Laboratory Animal Technology (Pinghu, China)) arrived at 6 weeks of age and were acclimatized for 7 days. All mice were maintained under specific pathogen-free (SPF) conditions (temperature, 24 ± 2 °C; humidity, 55 ± 10%) with a 12:12 light/dark cycle. Commercial chow (Jiangsu Xietong Organism, Nanjing, China) for SPF mice and autoclaved water were available ad libitum. All experimental procedures had been approved by the Animal Care and Use Committee of Jiangnan University.

In order to explore the effects of gut microbiota on MPTP-resistance of mice, all recipient mice were randomly assigned into four groups with 15 mice each in YM (young microbiota) and AM (aged microbiota) group, and 17 mice each in the YM + MPTP and AM + MPTP groups. Groups were treated as follows: (1) YM group: mice received microbiota from young mice for 7 days and remained untreated with MPTP; (2) AM group: mice received microbiota from aged mice for 7 days and remained untreated with MPTP; (3) YM + MPTP group: mice received microbiota from young mice for 7 days followed by MPTP treatment; (4) AM + MPTP group: mice

received microbiota from aged mice for 7 days followed by MPTP treatment.

FMT and MPTP Treatment

Donor mice and harvesting feces: male C57BL/6 J mice at the age of 7 weeks (young donors) or 23 months (aged donors) were used as donors for FMT in this study. Briefly, all donors were placed individually into sterile empty mouse cages and allowed to defecate freely. Fresh fecal pellets from donor mice were collected and dissolved in phosphate-buffered saline (PBS) immediately by homogenization (1 fecal pellet/ ~ 1 mL of PBS) once they were excreted. After centrifugation at 439 rcf for 10 min at 4 °C, the supernatant was collected and transferred to a clean tube and resuspended in sterilized PBS solution. After centrifugation at 7025 rcf for 5 min, the supernatant was discarded. The obtained microbiota was suspended in PBS containing 20% glycerin (10^8 CFU/ml, the OD value determined with a microplate reader at 600 nm) and stored at -80 °C until transplantation.

Recipient mice and FMT: Mice were first acclimated under SPF conditions for 7 days (day 1 ~ day 7). Recipient mice were administered by oral gavage with 200 µl of broad-spectrum antibiotics (1 mg/ml bacitracin (M06179, MERYER, Shanghai, China), 0.5 mg/ml gentamycin (405947, J&K, Shanghai, China), 0.2 mg/ml ciprofloxacin (M81368, MERYER, Shanghai, China), 1 mg/ml neomycin (HY-B0470, MedChemExpress, NJ, USA), 1 mg/ml penicillin (A70909, Sigma-Aldrich, St. Louis, MO, USA), 1 mg/ml metronidazole (HY-B0318, MedChemExpress, NJ, USA), 0.5 mg/ml ceftazidime (C3809, Sigma-Aldrich, St. Louis, MO, USA), 0.5 mg/ml vancomycin (V105495, Aladdin, Shanghai, China) and 2 mg/ml streptomycin (346858, J&K, Shanghai, China) dissolved in sterilized water) for 7 consecutive days (day 8 ~ day 14). Forty-eight hours after the seventh antibiotic gavage (day 15 ~ day 16), recipient mice were given 200 µl of the fecal bacterial stock daily for 7 consecutive days (day 17 ~ day 23) by gavage.

MPTP modeling: On day 24, the MPTP-induced PD model was initiated. Mice received 15 mg/kg (intraperitoneal injection, i.p.) MPTP-HCl (M0896, Sigma-Aldrich, St. Louis, MO, USA) every two hours for a total of four injections. The experimental timeline is shown in Fig. 2A.

Behavioral Analysis

The rotarod test was utilized to access mouse coordination of movement and balance. Mice were placed on a rotarod (ZB-200, Shanghai XinRuan Information Technology Co. LTD, Shanghai, China) and trained with a speed of 4 rpm for 300 s for 3 days before modeling (Fig. 2A, days 20 to 22). During the test (5 min), mice were placed on the accelerating rod with a speed of 4 to 40 rpm and the average time of latency to fall was recorded. Each mouse was tested for three rounds with 15 min intervals.

The pole-descent test and traction test were used to evaluate motor coordination and balance of mice as reported in previous studies [22]. After three consecutive behavioral training sessions on days 29 to 31, behavior tests were performed on day 32 (Fig. 2A). All tests were performed between 08:30 am and 12:00 pm (noon). In the pole-descent test, a rough pole, 50 cm long and 1 cm in diameter, with a 2 cm diameter ball fixed on the top was placed vertically in the cage. Mice were placed head down on the ball and the time taken to return to the cage was recorded. Pole tests for each mouse were conducted three times (15-min intervals) and the average time was calculated for further analysis. For the traction test, mice were hung by their forepaws on a horizontal wire. Scoring was conducted as follows: grabbing the wire with both front paws and both hind paws scored 4, grabbing the wire with two front paws and only one hind paw scored 3, grabbing the wire with only two front paws scored 2, and grabbing the wire with only one front paw scored 1. The test was conducted three times with 15 min intervals, and the average score was calculated.

Feces Sample Collection

16S rRNA assay and gas chromatography-mass spectrometry (GC–MS): mice were placed individually into empty autoclaved cages and allowed to defecate freely in the morning of the 8th day after MPTP treatment, then 6 to 10 pieces of feces per mouse were collected in individual sterile EP tubes on ice and stored at minus 80 °C immediately until further examination.

Intestinal Transit and Colon Length

Intestinal transit and colon length were evaluated before tissue collection on the thirty-second day. Thirty minutes before euthanizing the mice, a solution of 2.5% Evans blue (E2129, Sigma-Aldrich, St. Louis, MO, USA) in 1.5% methylcellulose (0.3 mL per animal) was intragastrically administered [23]. After euthanasia, intestinal transit was measured as the distance from the pylorus to the most distal point of migration. In addition, the length of the colon was measured.

Tissue Collection

Mice, under deep anesthesia with isoflurane (2 ~ 3%; S190815, Yuyuan, Shanghai, China), were transcardially perfused with ice-cold sterilized saline, and then were dissected. Fresh striatum, colon, hippocampus and serum of each mouse were obtained and rapidly stored at minus 80 °C before further analysis.

16S rRNA Sequencing

Fresh fecal pellets were collected from donor mice (young or old mice), and from recipient mice at the end of experiment (seven days after MPTP treatment). Detailed procedures for microbiota analysis are described as follows.

I. Extraction of genomic DNA: DNA was extracted using HiPure Stool DNA kits (D3141, Magen, Guangzhou, China) according to the manufacturer's protocol. The concentration and purity of DNA were measured by using a Thermo NanoDrop One (Thermo Fisher Scientific, Waltham, MA, USA).
II. Amplicon generation: 16S rRNA genes were amplified using specific primers (806R/515F) with a 12 bp barcode. Primers were synthesized by Invitrogen (Invitrogen, Carlsbad, CA, USA). PCR reactions (containing 25 µl 2 × Premix Taq (TaKaRa, Dalian, China), 1 µl each primer (10 µM) and 3 µl DNA (20 ng/µl) template)), in a total volume of 50 µl, were amplified by thermocycling: 5 min at 94 °C for denaturation, 30 cycles of 30 s denaturation at 94 °C, 30 s annealing at 52 °C, and 30 s extension at 72 °C, followed by 10 min final elongation at 72 °C. The PCR instrument was a Bio-Rad S1000 (Bio-Rad, Hercules, CA, USA).
III. PCR product detection, pooling and purification: the length and concentration of the PCR product were measured by 1% agarose gel electrophoresis. Samples with a bright main strip (e.g. 16S V4: 290-310 bp/16S V4V5: 400-450 bp) would be used for further analysis. PCR products were mixed in equidensity ratios according to the GeneTools analysis software (Version4.03.05.0, Syngene). After that, the mixture of PCR products was further purified with an E.Z.N.A. gel extraction kit (D2500, Omega, Norcross, Georgia, USA).
IV. Library preparation and sequencing: sequencing libraries were generated using an NEBNext Ultra II DNA Library Prep kit for Illumina (New England Biolabs, MA, USA) according to the manufacturer's instructions, and index codes were added. Library quality was determined with a Qubit 2.0 Fluorometer (Thermo Fisher Scientific, Waltham, MA, USA). Finally, the library was sequenced on an Illumina Nova6000 platform and 250 bp paired-end reads were generated (NeoBiotech, Guangzhou, China). 16S rRNA gene sequence libraries were generated using the V4 region on the Illumina MiSeq platform. Data analysis was performed using the QIIME v1.9.1 platform.

GC–MS Analysis

Fecal SCFAs were detected by GC–MS as previously reported [24]. First, 50 mg of fresh fecal pellets were ultrasonicated with 100 µl of sterile deionized water in a bath ultrasonicator for 5 min. They were then homogenized for another 2 min. After centrifugation at 4 °C, 20817 rcf for 15 min, 100 µl of the supernatant was acidified with 50 µl of sulfuric acid (50% v/v). After 10 min of vortexing and 2 min of standing, 225 µl of n-hexane was added to the above solution and the supernatant was obtained after centrifugation at 4 °C, 20817 rcf for 5 min [25, 26]. Standards, including acetic acid (A116165, Aladdin, Shanghai, China), propionic acid (P110443, Aladdin, Shanghai, China), butyric acid (B110439, Aladdin, Shanghai, China), isobutyric acid (I103521, Aladdin, Shanghai, China), valeric acid (V108269, Aladdin, Shanghai, China), isovaleric acid (I108280, Aladdin, Shanghai, China) were prepared freshly by diluting the stock solutions in n-hexane. The linear range of these SCFAs was measured by serial dilution of standards before detection. The gas chromatography–mass spectrometry was performed using a Trace 1300/Exactive GC apparatus (Thermo Fisher Scientific, Waltham, MA, USA) equipped with flame electron impact ionization and an Rtx-WAX column (30 m × 0.25 mm × 0.25 µm, Bellefonte, PA, USA).

Assessment of Neurotransmitters and Metabolites by High-Performance Liquid Chromatography (HPLC)

In order to test the contents of striatal neurotransmitters, including dopamine (DA), 5-hydroxytryptamine (5-HT) and their metabolites, including dihydroxy-phenylacetic acid (DOPAC), homovanillic acid (HVA) and 5-hydroxyindoleacetic acid (5-HIAA), HPLC, with a fluorescence detector (Waters 2475, Milford, MA, USA), a separation system (Waters 2695) and an Atlantis T3 column (150 mm × 4.6 mm, 5 µm, Waters) were used. For chromatographic conditions, ultra-pure water, acetonitrile and 0.01 M phosphate buffer (adjusted to pH 4 with phosphoric acid) were selected as mobile phases. For testing, fresh striatum was homogenized in 0.1 M perchloric acid (10 µl/mg striatum) by sonication on an ice bath. After centrifugation at 17949 rcf for 10 min at 4 °C, the supernatants were carefully collected and filtered through a 0.22 µm filter. Then, 25 µl of each sample was added into the column for testing. The standards, including DA (H8502, Sigma-Aldrich, St. Louis, MO, USA), 5-HT (H9523, Sigma-Aldrich, St. Louis, MO, USA), DOPAC (850217, Sigma-Aldrich, St. Louis, MO, USA), HVA (69673, Sigma-Aldrich, St. Louis, MO, USA) and 5-HIAA (H8876, Sigma-Aldrich, St. Louis, MO, USA), were prepared freshly by diluting the stock solutions in methanol. The linear range of these neurotransmitters was detected by serial dilution of standards before detection.

Western Blotting

Total protein was extracted by homogenizing 20 mg tissue in 200 µl radio immunoprecipitation assay lysis buffer (RIPA;

P0013C, Beyotime, Shanghai, China) with 2 µl phenylmethanesulfonyl fluoride (PMSF; ST506, Beyotime, Shanghai, China) and 4 µl phosphatase inhibitors (P1081, Beyotime, Shanghai, China). After centrifugation at 17949 rcf for 5 min at 4 °C, the supernatant was collected and protein concentration was determined with a BCA protein assay kit (BL521A, Biosharp, Hefei, China). The protein samples were boiled in a metal heat block for 15 min before further assay. Then, 30 µg of total protein was separated by sodium dodecyl sulfate–polyacrylamide electrophoresis-polyacrylamide gel electrophoresis (SDS-PAGE), and transferred to polyvinylidene difluoride membranes (PVDF; ISEQ00010, Millipore, Billerica, MA, USA). After blocking with 5% (w/v) skim milk (36120ES76, Yeasen Biotech, Hong Kong, China) dissolved in Tris-buffered saline containing 0.1% Tween-20 (P1379, Sigma-Aldrich, St. Louis, MO, USA) (TBST), the membrane was probed with the following antibodies: rabbit anti-tyrosine hydroxylase (TH, 1:1000; MAB152, Millipore, Billerica, MA, USA), rabbit anti-occludin (1:1000; 27260-1-AP, Proteintech Group, Chicago, IL, USA) and mouse anti-GAPDH (1:8000; 60001-1-Ig, Proteintech Group, Chicago, IL, USA) overnight at 4 °C. After washing with TBST, membranes were incubated with horseradish peroxidase (HRP)-conjugated goat anti-mouse or goat anti-rabbit IgG (1:1000; BA1050, Boster, Wuhan, China). After washing three times with TBST, protein bands were visualized with a chemiluminescent detection kit (P90720, Millipore, Billerica, MA, USA) and imaged by a Gel Image System (Bio-Rad, Hercules, CA, USA). Densitometry was performed by using ImageJ software (NIH, Bethesda, MA, USA). Data are shown as relative intensity following normalization to GAPDH.

Enzyme-Linked Immunosorbent Assay (ELISA)

For ELISA, total protein was extracted by homogenizing striatal tissue in 200 µl RIPA buffer (P0013C, Beyotime, Shanghai, China) with 2 µl phenylmethanesulfonyl fluoride (PMSF; ST506, Beyotime, Shanghai, China) and 4 µl phosphatase inhibitors (P1081, Beyotime, Shanghai, China). After centrifugation at 17949 rcf for 5 min at 4 °C, supernatant was collected and measured with a BCA protein assay kit (BL521A, Biosharp, Hefei, China). According to the manufacturer's instructions, striatal cytokine levels were assessed by commercial ELISA kits for TNF-α (FEK0527, Boster, Wuhan, China), IL-1β (EK0394, Boster, Wuhan, China), IL-10 (EK0417, Boster, Wuhan, China) and IL-6 (EK0411, Boster, Wuhan, China). Cytokine levels are presented as pg/ml protein.

Quantitative Real Time PCR (qRT-PCR)

Total RNA from the proximal colon or hippocampus was extracted with TRIzol (15596018, Invitrogen, Carlsbad, CA, USA) according to the manufacturer's instructions. The

Table 1 Primer sequences used for qRT-PCR

Gene ID	Gene name	Sequence (5'-3')	Fragment size (bp)
21926	Tnf-α	Forward: CGTCAGCCGATTTGCTATCT Reverse: CGGACTCCGCAAAGTCTAAG	206
16176	Il-1β	Forward: GCAACTGTTCCTGAACTCAACT Reverse: ATCTTTTGGGGTCCGTCAACT	89
16193	Il-6	Forward: TAGTCCTTCCTACCCCAATTTCC Reverse: TTGGTCCTTAGCCACTCCTTC	76
18126	iNos	Forward: CCTCCTCCACCCTACCAAGT Reverse: CACCCAAAGTGCTTCAGTCA	160
16173	Il-18	Forward: GACAGCCTGTGTTCGAGGAT Reverse: TGGATCCATTTCCTCAAAGG	188
16153	Il-10	Forward: GCTCTTACTGACTGGCATGAG Reverse: CGCAGCTCTAGGAGCATGTG	105
16189	Il-4	Forward: ATGCTGCTTCGACATCTCCT Reverse: AACCAATGCGAGATCCTGAC	196
21803	Tgf-β	Forward: CTCCCGTGGCTTCTAGTGC Reverse: GCCTTAGTTTGGACAGGATCTG	133
18260	Occludin	Forward: TTGAAAGTCCACCTCCTTACAGA Reverse: CCGGATAAAAAGAGTACGCTGG	129
19126	Cd133	Forward: GAAAAGTTGCTCTGCGAACC Reverse: CTCGACCTCTTTTGCAATCC	169
11461	β-Actin	Forward: CTGTATTCCCCTCCATCGTG Reverse: CCTCGTCACCCACATAGGAG	87
14433	Gapdh	Forward: AGGTCGGTGTGAACGGATTTG Reverse: TGTAGACCATGTAGTTGAGGTCA	123

purity and integrity of the obtained RNA (A260/A280 ratio was used as an indicator) assessed with a NanoDrop 1000 Spectrophotometer (Thermo Fisher Scientific, Waltham, MA, USA). Then, a two-step first-strand cDNA synthesis reaction was performed with a PrimeScript RT reagent kit (RR036A, TaKaRa, Otsu, Japan). The expression of mRNAs was determined by quantitative real-time PCR using SYBR Pre-mix Ex Taq II (RR820A, TaKaRa, Otsu, Japan) on a Light-Cycler 480 II (Roche, Basel, Switzerland). The mRNA quantification was calculated by the $2^{-\Delta\Delta Ct}$ method. The mRNA of the target gene was normalized to the Gapdh expression level or, in the case of *Cd133*, normalized to the *β-Actin* expression level. Primer sequences applied in this study are listed in the following (Table 1).

Immunofluorescence Staining

For immunofluorescence (IF) staining, mice were transcardially perfused with PBS followed by 4% paraformaldehyde (PFA) in PBS. Brain tissues were removed carefully and post-fixed in 4% PFA at 4 °C overnight, then transferred to 20% sucrose at 4 °C overnight and next to 30% sucrose at 4 °C overnight, and finally embedded in optimal cutting temperature compound (O.C.T. Compound, Tissue-Tek, USA). Each brain was cut into ten micrometer-thick coronal slices with a cryostat microtome (CM1950, Leica, Germany). Sections, containing the substantia nigra pars compacta (SNpc, from bregma -2.92 mm to -3.52 mm), were incubated with mouse anti-tyrosine hydroxylase (TH, 1:1000; MAB318, Millipore, Billerica, MA, USA) antibody after being blocked with 5% goat serum for 1 h at 37 °C, followed by incubation with fluorescein isothiocyanate (FITC)-conjugated goat anti-mouse IgG (1:1000; A0568, Beyotime, Shanghai, China). For glia analysis, slices containing the striatum were incubated with rabbit anti-Iba1 (1:1000; 019–19741, Wako, Osaka, Japan), or rabbit anti-GFAP (1:2000; Z033429, Dako, Glostrup, Denmark) primary antibodies after being blocked with 5% goat serum for 1 h at 37 °C. Subsequently, sections were incubated with appropriate secondary antibodies, FITC-conjugated goat anti-mouse IgG (1:1000; A0568, Beyotime, Shanghai, China) and Cy3-conjugated goat anti-rabbit IgG (1:1000; A0516, Beyotime, Shanghai, China) and counterstained with DAPI.

Brain slices containing the hippocampal dentate gyrus (DG) from bregma -1.46 mm to -2.46 mm were collected. Three representative slides (5 brain slices/slide, spaced 100 μm apart) were chosen for DCX staining. Briefly, DCX was labeled with a rabbit polyclonal antibody (1:250; 13925-1-AP, Proteintech Group, Chicago, IL, USA) and visualized using Cy3-conjugated goat anti-rabbit IgG, and nuclei were labeled with DAPI. Hippocampal DG imaging was then recorded with a fluorescence microscope (Olympus, Tokyo, Japan). Total DCX^+ cells in whole DG images were counted. The slices were imaged using an Axio Imager Z2 fluorescence microscope (Carl Zeiss LSM880, Zeiss, Germany).

Fig. 1 Comparison of the fecal microbiota of young and aged mice. ▶ **A** α-Diversity (Ace index) comparison of the gut microbiota. **B** Venn diagram of shared/unique OTUs in the fecal microbiota. **C** Principal component analyses (PCA) plots of the weighted UniFrac distances using the relative abundance of OTUs. Each point represents a sample from the young or aged group. **D** β-Diversity is depicted using a weighted Unifrac distance. **E** Overall representation of bacterial profiles by linear discriminant effect size (LEfSe) analysis; **F** histogram of bacterial taxa that significantly varied between the two groups (LDA > 3.0 and $p < 0.05$). **G** Relative abundance of *Ruminococcaceae UCG-014*, *Eubacterium xylanophilum* group and *Lactobacillus* at the genus level based on 16S rRNA sequencing. N = 6 in the young group and n = 4 in the aged group. *: $P < 0.05$ and **: $P < 0.01$

Nissl Staining

Sections containing the SNpc were washed twice with distilled water for 2 min each wash. After that, sections were incubated with Cresyl violet stain (G1430, Solarbio, Beijing, China) at room temperature for 1 h. The sections were rinsed twice with distilled water, followed by ~ 2 min differentiation with Nissl differentiation solution (G1430, Solarbio, Beijing, China). Differentiation was terminated when the background was close to colorless or light blue). The sections were dehydrated with ethanol, cleared in xylene and sealed with neutral gum. Slices were placed under a microscope for observation and imaging. Nissl-stained body areas in the SNpc were calculated by ImageJ software.

Immunohistochemistry

After antigen retrieval (45 min at 99 °C), brain sections containing the hippocampal dentate gyrus were treated with 3% H_2O_2 (Reagent 1 in PV-9005, ZSGB-Bio, Beijing, China) at room temperature for 20 min. After washing in PBS three times for 3 min each, sections were blocked with 5% goat serum (SL038, Solarbio, Beijing, China) at 37 °C for 30 min and then incubated overnight at 4 °C with rabbit anti-Ki67 antibody (1:500, ab15580, Abcam, UK). Antibody binding was amplified with reaction enhancement solution (Reagent 2 in PV-9005, ZSGB-Bio, Beijing, China) at 37 °C for 20 min. After washing in PBS three times for 3 min each, sections were subsequently incubated with biotinylated goat anti-rabbit antibody (PV-9000, ORIGENE, China) at room temperature for 20 min. After washing in PBS three times for 3 min each, the sections were subjected to an AEC staining kit (ZLI-9036, ORIGENE, China) at room temperature for 5–8 min until color developed. Finally, water-soluble sealant (AR1018, Boster, Wuhan, China) was used to seal the slides. Positive antibody expression in the sections was dark brown and all sections were viewed using digital slide scanners

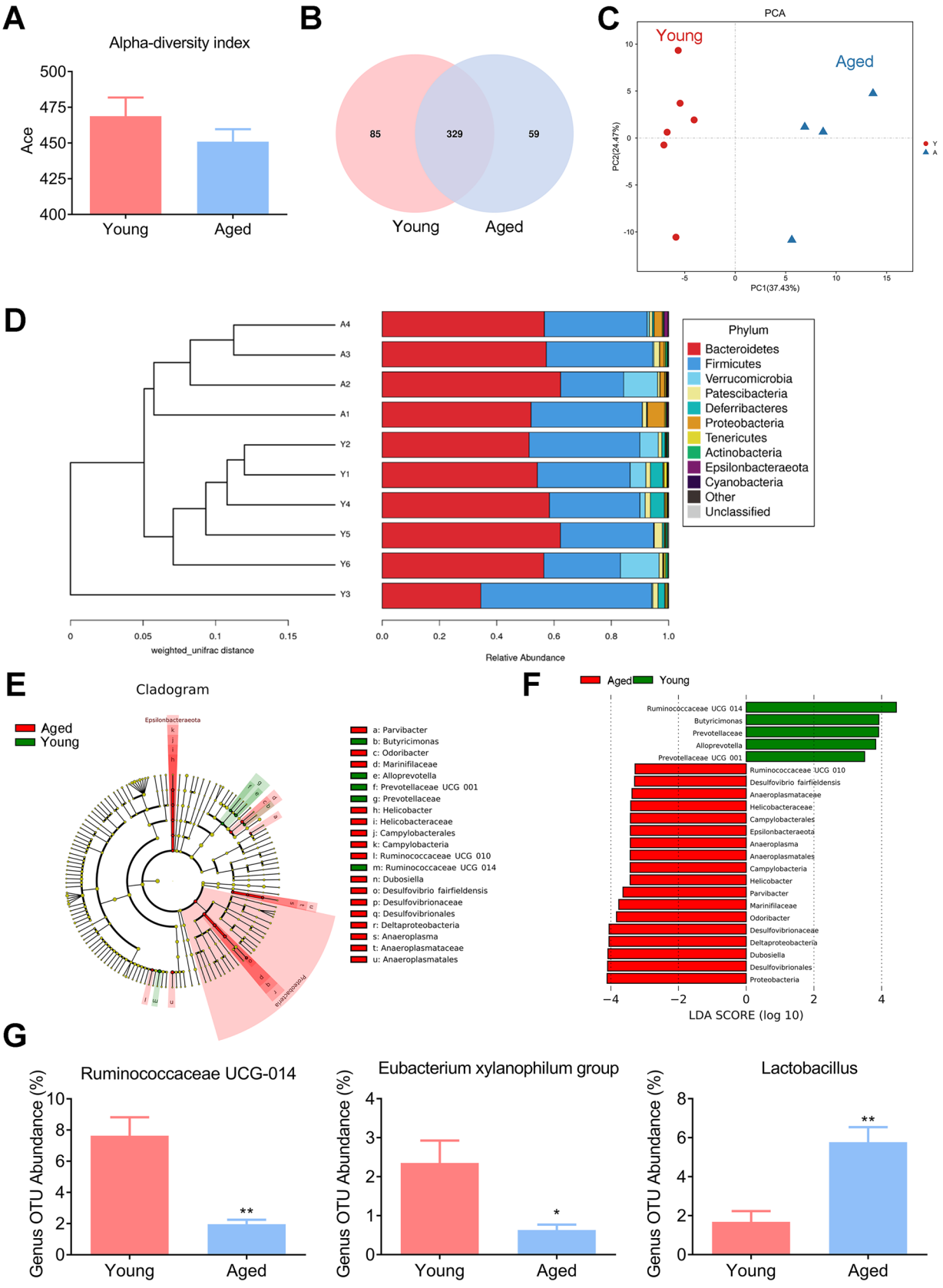
A
Alpha-diversity index
Ace
500
475
450
425
400
Young
Aged
B
85
329
59
Young
Aged
C
PCA
Young
Aged
PC2(24.47%)
PC1(37.43%)
D
A4
A3
A2
A1
Y2
Y1
Y4
Y5
Y6
Y3
weighted_unifrac distance
Relative Abundance
Phylum
Bacteroidetes
Firmicutes
Verrucomicrobia
Patescibacteria
Deferribacteres
Proteobacteria
Tenericutes
Actinobacteria
Epsilonbacteraeota
Cyanobacteria
Other
Unclassified
E
Cladogram
Aged
Young
Epsilonbacteraeota
Proteobacteria
a: Parvibacter
b: Butyricimonas
c: Odoribacter
d: Marinifilaceae
e: Alloprevotella
f: Prevotellaceae UCG 001
g: Prevotellaceae
h: Helicobacter
i: Helicobacteraceae
j: Campylobacterales
k: Campylobacteria
l: Ruminococcaceae UCG 010
m: Ruminococcaceae UCG 014
n: Dubosiella
o: Desulfovibrio fairfieldensis
p: Desulfovibrionaceae
q: Desulfovibrionales
r: Deltaproteobacteria
s: Anaeroplasma
t: Anaeroplasmataceae
u: Anaeroplasmatales
F
Aged
Young
Ruminococcaceae UCG 014
Butyricimonas
Prevotellaceae
Alloprevotella
Prevotellaceae UCG 001
Ruminococcaceae UCG 010
Desulfovibrio fairfieldensis
Anaeroplasmataceae
Helicobacteraceae
Campylobacterales
Epsilonbacteraeota
Anaeroplasma
Anaeroplasmatales
Campylobacteria
Helicobacter
Parvibacter
Marinifilaceae
Odoribacter
Desulfovibrionaceae
Deltaproteobacteria
Dubosiella
Desulfovibrionales
Proteobacteria
LDA SCORE (log 10)
G
Ruminococcaceae UCG-014
Genus OTU Abundance (%)
Young
Aged
Eubacterium xylanophilum group
Genus OTU Abundance (%)
Young
Aged
Lactobacillus
Genus OTU Abundance (%)
Young
Aged

(Pannoramic MIDI, Hungary). The number of $Ki67^+$ cells in the dentate gyrus of the hippocampus was counted using CaseViewer software.

Statistical Analyses

Differences among groups were assessed using one-way ANOVA followed by a Bonferroni's post hoc test when variance was uniform, and Dunnett's T3 analysis when variance was not uniform, by using SPSS 25.0 software. Statistical analyses were performed using GraphPad Prism 6.0 software (GraphPad Software, Inc. La Jolla, CA, USA). $P < 0.05$ was set as the threshold for significance ($^*P < 0.05$, $^{**}P < 0.01$ and $^{***}P < 0.001$).

Results

Gut Microbiota Diversity Between Aged and Young Mice

Given the recent evidence that the composition and diversity of gut microbiota varies with age [27], we first determined whether gut microbiota displayed different characteristics between young mice (7 weeks) and aged mice (23 months). Alpha and beta diversity analysis offer a comprehensive view of gut microbiota and focus on the abundance and diversity, as well as distribution of gut microbiota. The alpha diversity of gut microbiota was indicated by the Ace index and Venn diagram, representative of community richness and principal components. The Ace index tended to be slightly decreased in aged mice, but there was no statistical difference between the two groups (Fig. 1A). We further established a Venn diagram, based on shared operational taxonomic units (OTUs), to observe the composition of gut microbiota. The number of shared bacterial genera in the two groups was 329. There were 85 and 59 unique OTUs in the young and aged groups, respectively, indicating that a distinct composition of the gut microbiota exists in mice at different ages (Fig. 1B). Principal components (PCs) 1 and 2 explain 37.43% and 24.47% of the variance, respectively. Principal component analyses (PCA) of the UniFrac distance revealed that significant separation occurred between the two groups, suggesting the degree of similarity of gut microbiota, in terms of both the presence and relative abundance of bacterial taxonomies, changes in profile with host age (Fig. 1C). Beta diversity was further evaluated with UPGMA clustering. A clear separation between the two groups is shown in Fig. 1D, indicating differences in microbial composition between the two groups of mice. In addition, linear discriminant analysis effect size (LEfSe) revealed that the composition of the gut microbiota between young and aged donor mice had significant differences, as shown in the cladogram and histogram. LEfSe analysis also showed that a higher abundance of the *Proteobacteria* phylum and its lower taxonomic level were notable in the aged donor mice (Fig. 1E and F). Remarkably, we found that significant differences existed in aged mice and involve decreases in *Ruminococcaceae UCG-014*, which are potential SCFA-producing bacteria [28–30] and *Eubacterium xylanophilum* group [31], and an increase in *Lactobacillus* (known as beneficial genera/species [32]) (Fig. 1G). These results, in line with previous studies showing that differences exist between aged and young gut microbiota populations [20], indicate that the gut microbiota undergo age-related changes with the host aging process.

FMT from Aged Mice to MPTP-Treated Mice Improves Locomotor Function

To assess the influence of microbiota donor age as a factor on the ability of gut microbiota to confer resistance to MPTP, we transplanted gut microbiota from young (7 weeks) or aged (23 months) donor mice into adult recipient mice (8 weeks), followed by MPTP injection (Fig. 2A). Body weights were monitored daily and behavioral tests were performed. MPTP injection markedly decreased the body weight in both YM + MPTP and AM + MPTP groups (Fig. 2B), but body weights returned to normal levels on the 4th day after MPTP administration. The pole test, rotarod test and traction test were used to measure motor functions. YM + MPTP mice had a longer descent time and a decreased fall latency than YM mice due to the toxicity of MPTP. AM + MPTP mice exhibited a significantly shorter descent time and an extended running duration than YM + MPTP mice, suggesting that FMT from aged mice could improve the locomotor function of adult mice (Fig. 2C). However, in the traction test, there was no difference in mice among four groups (Fig. 2D). These results indicate that FMT from aged mouse donors was able to partially resist the motor dysfunction caused by MPTP.

FMT from Aged Donors Increases Neurotransmitters in the Striatum of PD Mice

PD is characterized by the degeneration of dopaminergic neurons, resulting in reduced striatal dopamine (DA) levels, leading to motor and non-motor symptoms. As expected, striatal DA levels were dramatically decreased in MPTP-treated mice (mice in YM + MPTP and AM + MPTP groups) compared with control mice (mice that received FMT from young or aged mice followed by saline injection, denoted YM mice and AM mice, respectively) (Fig. 3A), and striatal DA did not differ between AM + MPTP mice and YM + MPTP mice, indicating FMT could not inhibit MPTP-induced DA

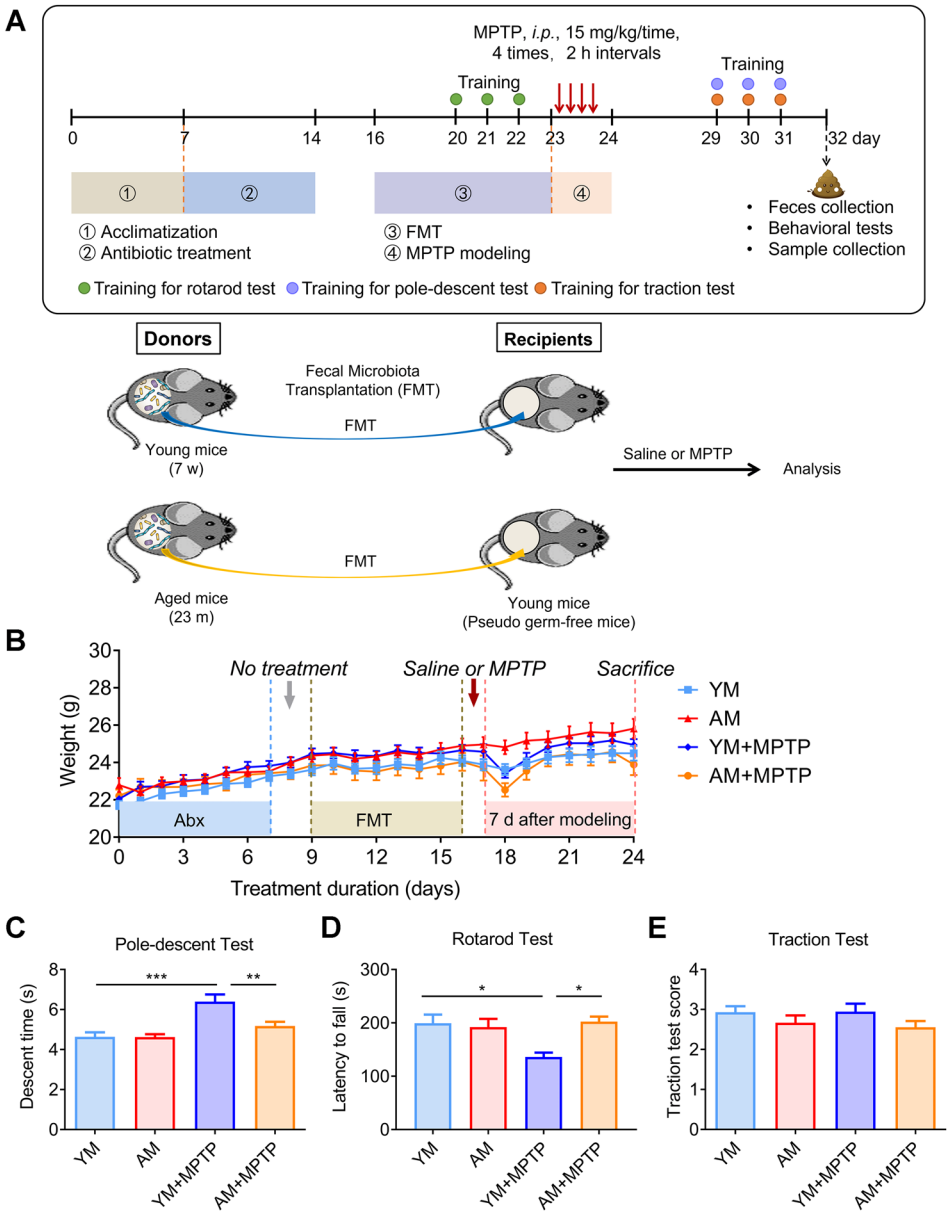

Fig. 2 Effects of FMT from young and aged donors on body weight and locomotor functions. **A** Schematic representation of the procedure of animal experiments and schematic diagram of the FMT experiment. **B** Changes in body weight over time. **C** Pole descent test. **D** Rotarod test. **E** Traction test. For **C** and **E** tests: N = 10 in the YM and AM groups, n = 12 in the YM + MPTP and AM + MPTP groups; For D test: N = 5 in each group. *: $P < 0.05$, **: $P < 0.01$ and ***: $P < 0.001$

reduction, regardless of fecal microbiota donor age. Also, no significant difference in DA levels was observed between YM and AM mice (Fig. 3A), suggesting young microbiota and aged microbiota do not cause different effects on DA levels. Moreover, striatal DOPAC/DA and HVA/DA ratios increased in MPTP-treated mice (YM + MPTP mice and AM + MPTP mice) compared with control YM mice and AM mice, respectively, indicating increased DA turnover caused by MPTP. Intriguingly, AM + MPTP mice exhibited decreased DOPAC/DA and HVA/DA ratios, suggesting a reduction in dopaminergic turnover rate of aged microbiota in PD mice. There was no difference between YM and AM mice, indicating no effect of aged microbiota on DA turnover in control mice (Fig. 3B, C).

5-HT is another key neurotransmitter and signaling molecule that might be associated with the ability of gut microbiota to increase neuroactive metabolites [33]. Similarly, there was a clear decrease in 5-HT levels in MPTP mice (both YM + MPTP and AM + MPTP mice) compared with control mice (YM mice and AM mice). However, the 5-HT levels in AM + MPTP mice were significantly higher than that in YM + MPTP mice. Unexpectedly, AM mice showed a significant increase of 5-HT than YM mice (Fig. 3D), suggesting aged microbiota promote 5-HT production in recipient mice. Compared to control YM and AM mice, the turnover of 5-HT was increased in MPTP-treated mice (both YM + MPTP mice and AM + MPTP mice) (Fig. 3E). Unlike the DA turnover, 5-HT turnover shown no difference

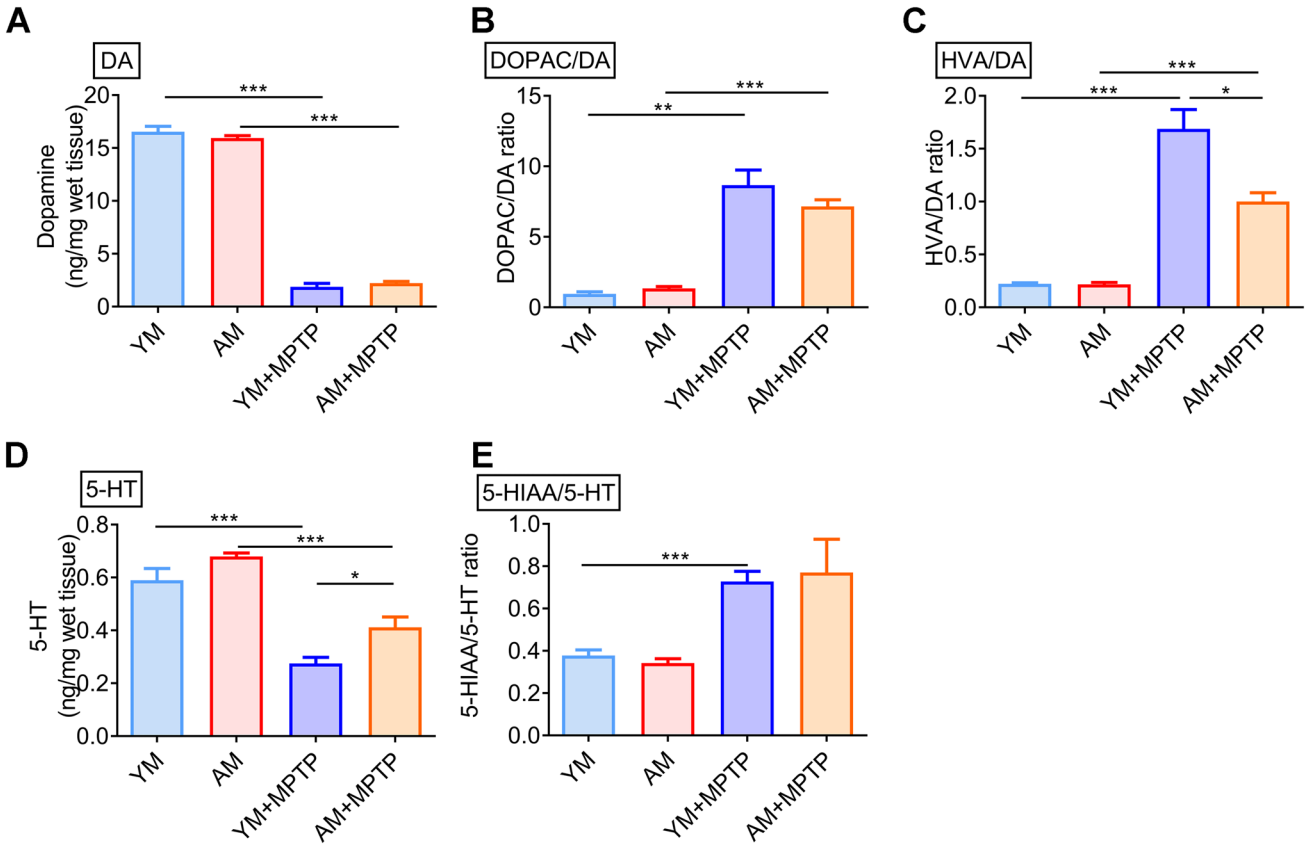

Fig. 3 Effects of FMT from young and aged mice on neurotransmitters and their metabolism. **A** Striatal DA concentration. **B** Ratio of DOPAC/DA. **C** Ratio of HVA/DA. **D** Striatal 5-HT concentration. **E** Ratio of 5-HIAA/5-HT. N = 7 in the YM group, n = 6 in the AM group, n = 9 in the YM + MPTP and AM + MPTP groups. *: $P < 0.05$; **: $P < 0.01$ and ***: $P < 0.001$

between YM + MPTP mice and AM + MPTP mice. Therefore, FMT from aged mice could ameliorate the reduction of striatal 5-HT content induced by MPTP and slow down the turnover of DA.

FMT from Aged Donors Suppresses the Loss of Dopaminergic Neurons and Does Not Affect TH Expression in MPTP-Induced PD Mice

The number of dopaminergic neurons in the SNpc was examined to evaluate the effect of aged microbiota on PD mice by immunofluorescence and Nissl staining. As we expected, the MPTP-treated groups (YM + MPTP mice and AM + MPTP mice) showed a sharp loss of TH-positive (TH^+) cells, when compared with control mice (YM mice and AM mice). However, AM + MPTP mice had 53.9% less loss in the number of TH^+ cells than YM + MPTP mice (Fig. 4A and B). Similarly, the percentage of Nissl body area dramatically decreased in the MPTP-treated groups (Fig. 4C–D). However, AM + MPTP mice had a larger amount of Nissl-stained bodies when compared to that in YM + MPTP mice. These findings suggest that aged microbiota suppresses the loss of dopaminergic neurons caused by MPTP toxicity. Additionally, striatal TH expression was dramatically decreased in MPTP-treated mice (YM + MPTP mice and AM + MPTP mice) compared to control mice (YM mice and AM mice) (Fig. 4E and F). Yet, no increase in TH expression was found in AM + MPTP mice when compared with YM + MPTP mice, implying that FMT from aged donors had no effect on striatal TH expression.

FMT Modulates Gut Microbiota in PD Mice

The composition of gut microbiota of mice after 21 days of FMT were analyzed by using 16S rRNA gene sequencing. In order to explore the effect of FMT from aged mice on PD mice, alpha and beta diversities of gut microbiota were performed to analyze the abundance, diversity and distribution of gut microbiota. The Shannon index and Simpson index, two indices of alpha diversity, comprehensively reflect the richness and evenness of species. Unexpectedly, the Shannon and Simpson indices indicated that the intracommunity variations were similar among the four groups (Fig. 5A, B). We further evaluated the extent of similarity of gut microbial

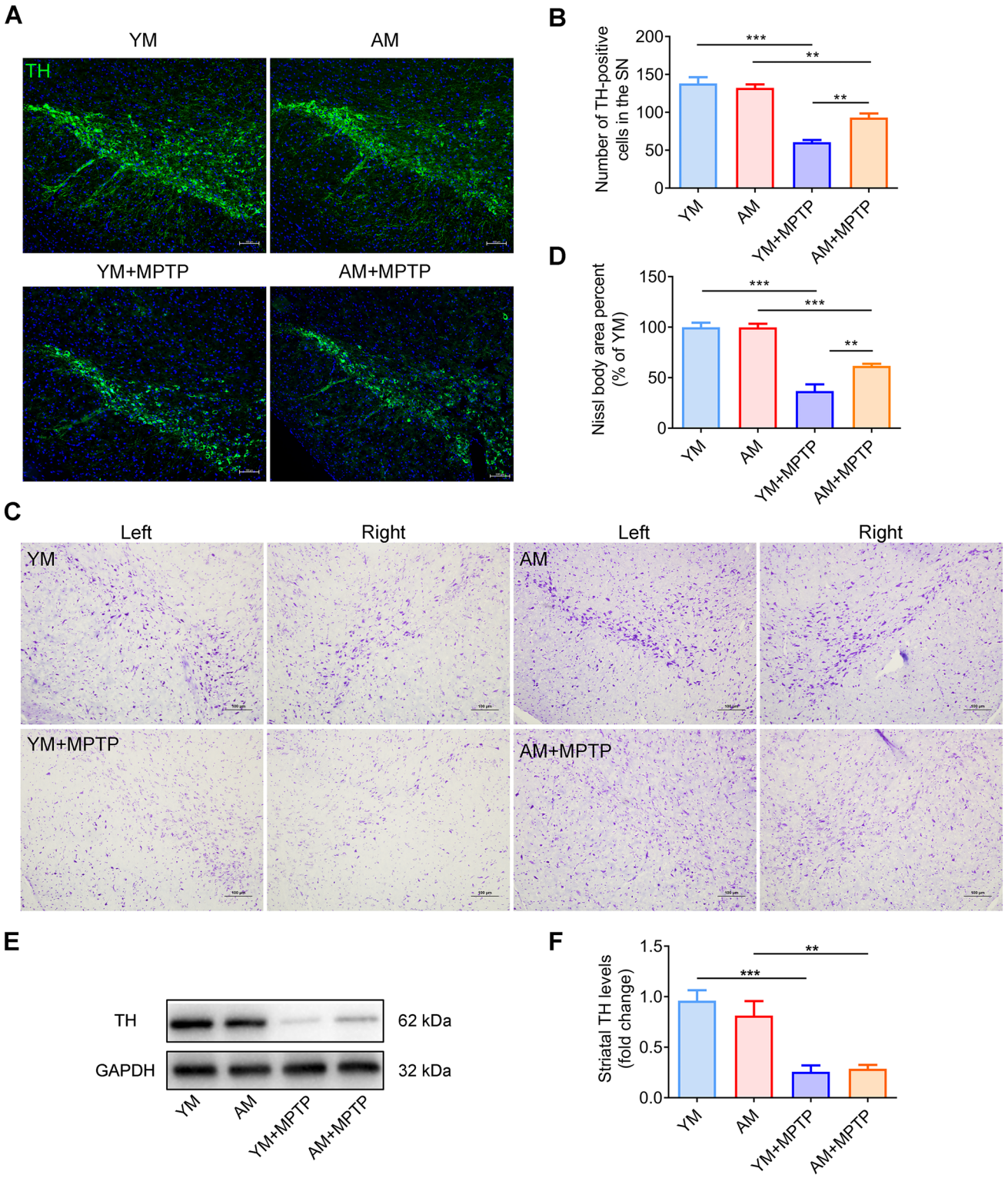

Fig. 4 Effect of FMT from young and aged mice on brain dopaminergic neurons and TH expression. **A** Immunostaining of TH in the SNpc region of mouse brains in the different groups. **B** Quantification of TH-positive neuronal cell bodies with representative immunofluorescence images of SNpc sections. **C** Nissl staining of the SN of mice in different groups under the microscope. **D** Quantification of Nissl body area percent, as exhibited in (**C**). N = 5 in each group. Scale bar: 100 μm. **E** Western blotting for TH protein expression. **F** Quantification of TH expression in the striatum. N = 7 in each group. *: $P < 0.05$; **: $P < 0.01$ and ***: $P < 0.001$

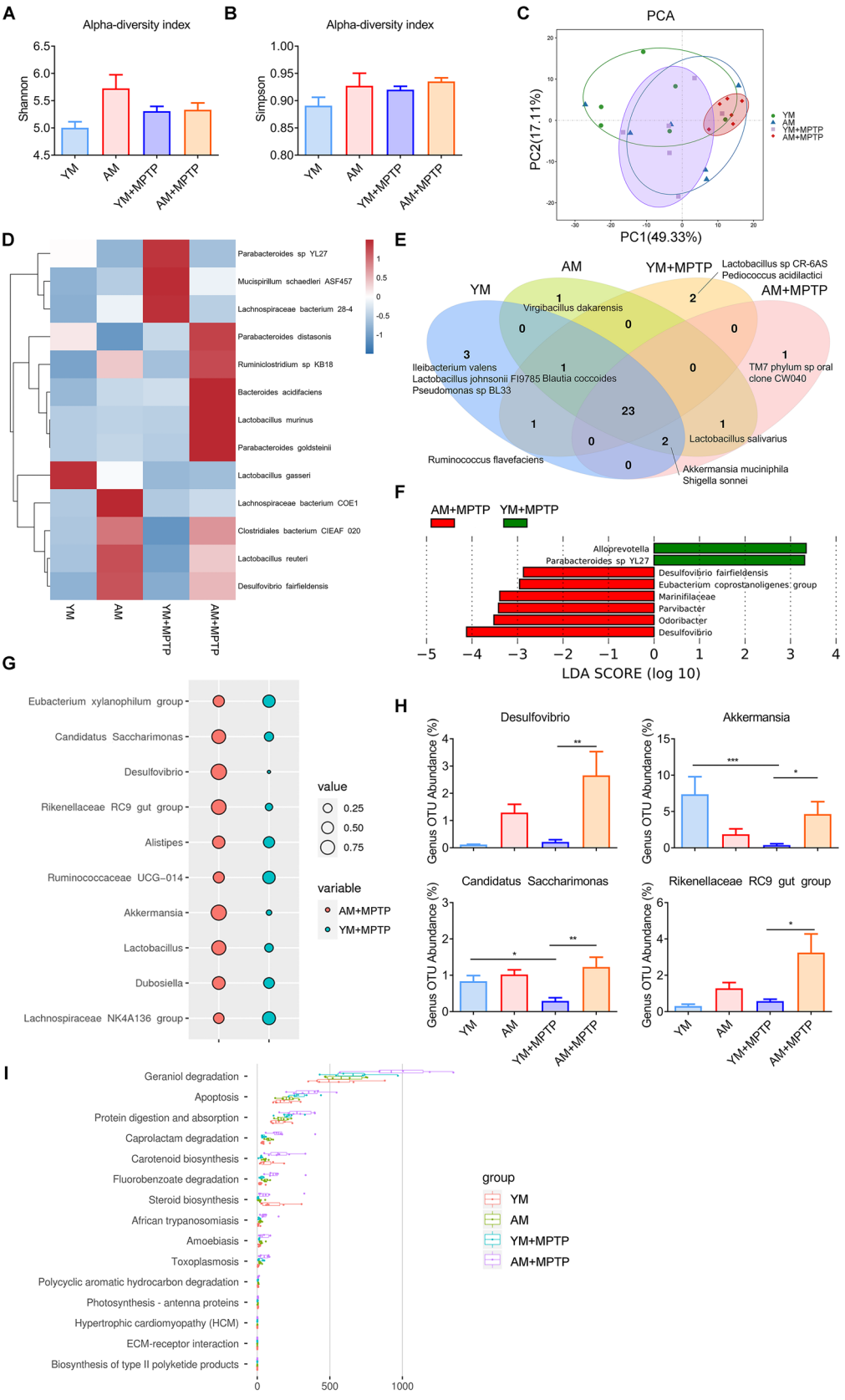
A
Alpha-diversity index
Shannon
YM
AM
YM+MPTP
AM+MPTP
B
Alpha-diversity index
Simpson
C
PCA
PC2(17.11%)
PC1(49.33%)
D
Parabacteroides sp YL27
Mucispirillum schaedleri ASF457
Lachnospiraceae bacterium 28-4
Parabacteroides distasonis
Ruminiclostridium sp KB18
Bacteroides acidifaciens
Lactobacillus murinus
Parabacteroides goldsteinii
Lactobacillus gasseri
Lachnospiraceae bacterium COE1
Clostridiales bacterium CIEAF 020
Lactobacillus reuteri
Desulfovibrio fairfieldensis
E
Virgibacillus dakarensis
Lactobacillus sp CR-6AS
Pediococcus acidilactici
Ileibacterium valens
Lactobacillus johnsonii FI9785 Blautia coccoides
Pseudomonas sp BL33
TM7 phylum sp oral clone CW040
Lactobacillus salivarius
Ruminococcus flavefaciens
Akkermansia muciniphila
Shigella sonnei
F
AM+MPTP
YM+MPTP
Alloprevotella
Parabacteroides sp YL27
Desulfovibrio fairfieldensis
Eubacterium coprostanoligenes group
Marinifilaceae
Parvibacter
Odoribacter
Desulfovibrio
LDA SCORE (log 10)
G
Eubacterium xylanophilum group
Candidatus Saccharimonas
Desulfovibrio
Rikenellaceae RC9 gut group
Alistipes
Ruminococcaceae UCG-014
Akkermansia
Lactobacillus
Dubosiella
Lachnospiraceae NK4A136 group
value
0.25
0.50
0.75
variable
AM+MPTP
YM+MPTP
H
Desulfovibrio
Akkermansia
Candidatus Saccharimonas
Rikenellaceae RC9 gut group
Genus OTU Abundance (%)
I
Geraniol degradation
Apoptosis
Protein digestion and absorption
Caprolactam degradation
Carotenoid biosynthesis
Fluorobenzoate degradation
Steroid biosynthesis
African trypanosomiasis
Amoebiasis
Toxoplasmosis
Polycyclic aromatic hydrocarbon degradation
Photosynthesis - antenna proteins
Hypertrophic cardiomyopathy (HCM)
ECM-receptor interaction
Biosynthesis of type II polyketide products
group
YM
AM
YM+MPTP
AM+MPTP

◂**Fig. 5** Effects of FMT from young and aged mice on fecal bacterial diversity, composition and functionality of the gut microbiota in MPTP-treated mice. Analysis of α-diversity-predicted diversity of gut microbiota by **A** Shannon index and **B** Simpson index. **C** Principal component analyses (PCA) plots of the weighted UniFrac distances using the relative abundance of OTUs. The position and distance of each points indicates the degree of similarity in terms of both the presence and relative abundance of bacterial taxonomies. **D** Heatmap showing 16S rRNA expression pattern in different treatment groups. Bacterial species are shown on the right and the heatmap scale is -1.5 ~ 1.5. **E** Venn diagram of shared/unique species in the fecal microbiota. **F** LEfSe was calculated to assess the functions of the gut microbiota that more strongly discriminated YM + MPTP and AM + MPTP mice. **G** Top 10 biomarkers at the genus level between YM + MPTP and AM + MPTP groups are presented in the bubble plot. **H** Relative abundance of fecal microbiota (*Desulfovibrio*, *Akkermansia*, *Candlcatus Saccharimonas* and *Rikenellaceae RC9 gut group*) changed significantly at the genus level based on 16S rRNA sequencing. **I** Functional prediction analyses based on OTU species annotation and abundance information in microbiota among the four treatment groups (those with abundance > 1% are presented). N = 6 in each group. *: $P < 0.05$; **: $P < 0.01$ and ***: $P < 0.001$

communities among the four groups by using PCA based on the weighted UniFrac distance. A distinct separation of microbiota community was observed between AM + MPTP (red) and YM + MPTP (purple) groups, indicating that the overall structures of the bacterial communities between these two groups were significantly different (Fig. 5C). We explored the composition of gut microbiota to identify the potential bacterial groups responsible for microbial alterations. As previously reported [34, 35], the composition of gut microbiota strongly shifted in the MPTP-treated groups compared to the MPTP-untreated groups (YM vs. YM + MPTP; AM vs. AM + MPTP), as shown in the heatmap (Fig. 5D). Interestingly, changes in gut bacterial communities were more subtle between YM + MPTP mice and AM + MPTP mice (Fig. 5D). We also established a Venn diagram based on shared taxa to evaluate the overall structure of gut microbiota. We observed 26 bacterial taxa that were shared between YM and AM mice, and 23 bacterial taxa between YM + MPTP and AM + MPTP mice. Additionally, only one taxon (*Virgibacillus dakarensis*) was found in AM mice, while three taxa (*Ileibacterium valens*, *Lactobacillus johnsonii Fl9785*, *Pseudomonas sp BL33*) were found in YM mice. Two bacterial taxa (*Lactobacillus sp CR-6AS*, *Pediococcus acidilactici*) and only one taxon (*TM7 phylum sp oral clone CW040*) were found in the fecal microbiota of YM + MPTP and AM + MPTP mice, respectively. Unlike *Ruminococcus flavefaciens*, which was shared only in mice receiving FMT with young microbiota, *Lactobacillus salivarius* was shared between AM and AM + MPTP mice. We also observed that *Blautia coccoides* was presented in all groups except in AM + MPTP mice. Similarly, *Akkermansia muciniphila* and *Shigella sonnei* were presented in all groups except in YM + MPTP mice (Fig. 5E). The taxa that discriminated between YM + MPTP and AM + MPTP mice were filtered by using the LEfSe method, and their effect sizes were also calculated to further analyze the effect of young or aged microbiota on the composition of the fecal microbiota of PD mice. There was an overrepresentation of *Alloprevotella* and *Parabacteroides sp YL27* in YM + MPTP mice, and a relatively higher abundance of the species *Desulfovibrio fairfieldensis*, the genera *Eubacterium coprostanoligenes* group, *Parvibacter*, *Desulfovibrio* and *Odoribacter*, and the family *Marinifilaceae* in AM + MPTP mice. The biomarkers of the top 10 genera distinguishing between the YM + MPTP group and AM + MPTP group are shown in Fig. 5G. Notably, *Desulfovibrio*, *Akkermansia*, *Candlcatus Saccharimonas* and *Rikenellaceae RC9 gut* group were significantly enriched in the AM + MPTP group compared with YM + MPTP mice (Fig. 5H). Functional prediction analyses revealed significant differences between YM + MPTP and AM + MPTP groups, which were associated with geraniol degradation, apoptosis, protein digestion and absorption, caprolactam degradation, carotenoid biosynthesis and fluorobenzoate degradation (Fig. 5I). These findings suggest that the response of aged microbiota to MPTP treatment is different from that of young microbiota.

FMT from Aged Donors Promotes the Restoration of Normal Fecal SCFA Levels in Mice

Given gut microbiota metabolites, for example, SCFAs, have been linked to the pathophysiology of PD, GC–MS was used to examine the fecal concentrations of certain SCFAs (including acetic acid, propionic acid, butyric acid, isobutyric acid, valeric acid and isovaleric acid). The aim was to evaluate differences of fecal SCFA concentrations among the four treatment groups and provide clues about the relationship between fecal SCFAs and pathological features associated with PD. Among the tested fecal SCFAs, butyric acid content was altered to the greatest extent, a significant increase was found in YM + MPTP mice compared to control YM mice and AM + MPTP mice, which did not differ from AM mice (Fig. 6A). Similar differences were found for fecal concentrations of iso-SCFAs (isobutyric acid and isovaleric acid) (Fig. 6B–C) and valeric acid concentration (Fig. 6D). The same trends were also observed for propionic acid or acetic acid (Fig. 6E–F).

Furthermore, we performed correlation analyses between SCFAs and three highly affected parameters associated with PD disease progression, namely motor dysfunction (pole test), striatal 5-HT concentrations and DA metabolism (HVA/DA ratios). Remarkably, we observed significant positive correlations between SCFAs and motor dysfunction, as well as between SCFAs and DA metabolism. However, no significant association was found between SCFAs and striatal 5-HT. Taken together, these data suggest that SCFAs might play a key role in mediating host pathophysiological changes in PD mice receiving FMT with aged microbiota.

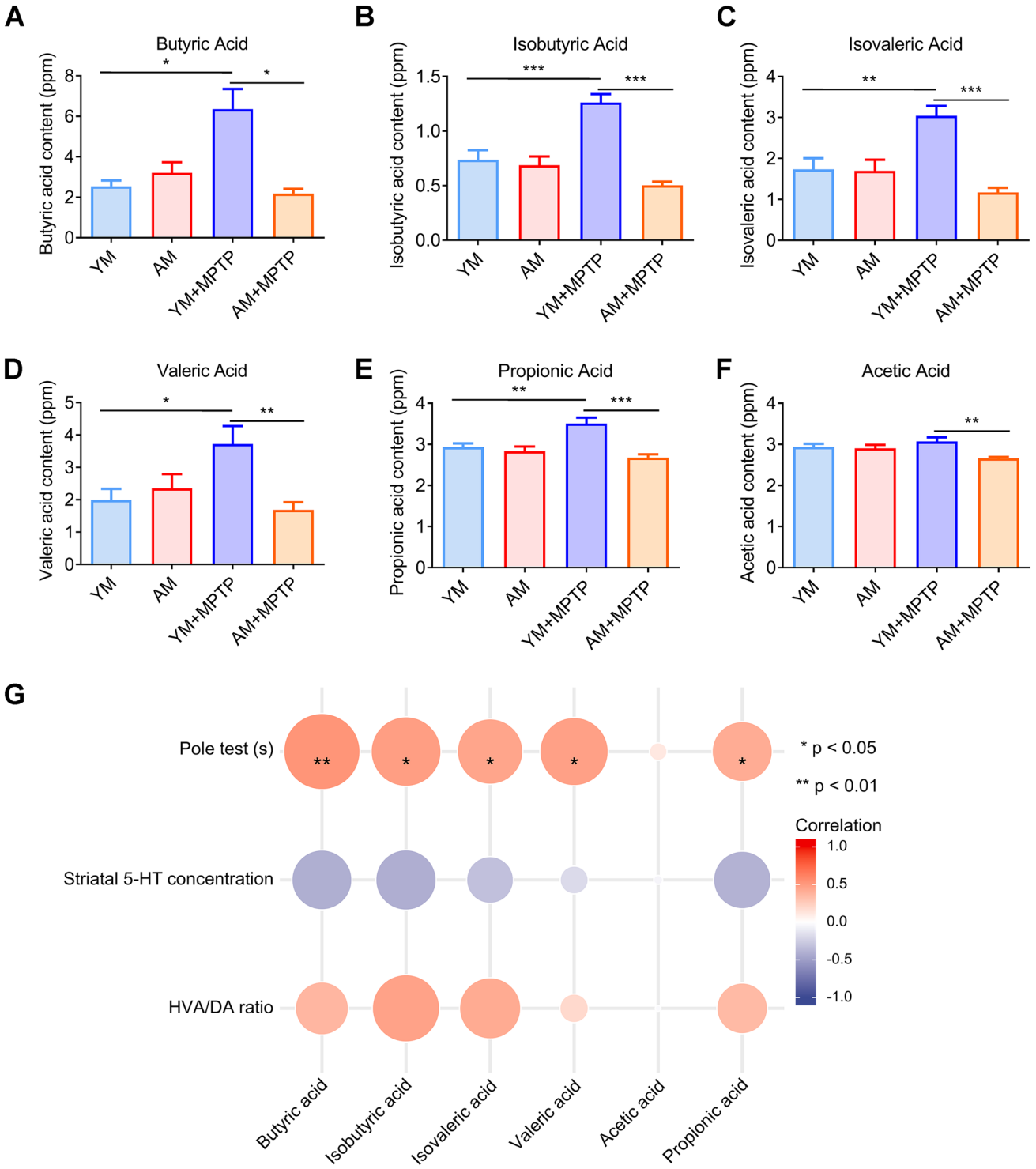

Fig. 6 Effects of FMT from young and aged mice on fecal SCFA levels. **A** Contents of fecal butyric acid. **B** Contents of fecal isobutyric acid. **C** Contents of fecal valeric acid. **D** Contents of fecal isovaleric acid. **E** Contents of fecal propionic acid. **F** Contents of fecal acetic acid. **G** Correlation between SCFAs and PD phenotype among the YM, AM, YM + MPTP and AM + MPTP groups. N = 8 in each group. *: $P < 0.05$; **: $P < 0.01$ and ***: $P < 0.001$

FMT from Aged Donors Does Not Alleviate Striatal Neuroinflammation

To elucidate the role of FMT from aged mice in the number of glial cells in the present study, we examined glial cells in the striatum by immunofluorescence staining for Iba1 (microglia marker). A higher number of Iba1-positive ($Iba1^+$) microglia was observed in the striatum of MPTP-treated mice (YM + MPTP mice and AM + MPTP mice) compared with control mice (YM mice and AM mice), but numbers were comparable between AM + MPTP mice and YM + MPTP mice (Fig. 7A and C). The mean fluorescence intensity of GFAP in the striatal astrocytes increased in MPTP-treated mice compared with control mice, with astrocytes in AM + MPTP mice tending to be slightly, but not significantly increased compared with YM + MPTP mice (Fig. 7B and D).

To further confirm whether neuroinflammation is involved in aged microbiota-mediated neuroprotection in PD mice, we characterized the striatal cytokines, including TNF-α, IL-1β, IL-10 and IL-6, by ELISA. Of note, no differences among the four treatment groups was observed (Fig. 7E–H). Therefore, these results together indicate that FMT from aged donors does not trigger phenotypic changes in striatal glia cells or affect striatal cytokine expression of PD mice.

FMT from Aged Donors Does Not Affect Levels of Colonic Inflammation

Several aspects of intestinal dysfunction are presented in PD. However, there was no difference in the transport distance of Evans blue dye in the small intestine among the four groups (Fig. 8A). YM + MPTP mice showed a reduction in colon length compared with that in YM mice (Fig. 8B). However, there was no change in colon length between YM + MPTP and AM + MPTP mice, implying that any effect of microbiota on colon length was not dependent on microbiota donor age.

The association between intestinal permeability and inflammation is bidirectional and remains relevant. As is well known, dysbiotic microbiota may reduce epithelial barrier proteins, such as claudin-1 and occludin, by secreting metabolites, and disrupt cell-to-cell connections, which compromises intestinal permeability [36]. In order to evaluate gut permeability, we characterized the expression of tight junction proteins, including claudin-1 and occludin, by western blotting and qRT-PCR. Yet, neither occludin (Fig. 8C–E) nor claudin-1 (data not shown) was altered in the colons of mice from any of the four groups. Furthermore, the expression of inflammatory cytokines, including *Tnf-α*, *Il-1β*, *Il-6*, *iNos*, *Il18*, *Il10*, *il4* and *Tgf-β*, showed no significant change among all groups (Fig. 8F). These results confirm that FMT from an aged host does not affect intestinal barrier permeability or the intestinal inflammatory response caused by MPTP treatment.

FMT from Aged Donors Triggers Neurogenesis in the Hippocampus

Different studies have shown the influence of gut microbiota in neurogenesis [6, 37–39]. Inspired by a study from Parag Kundu and coworkers in 2019, showing neurogenesis and pro-longevity signaling in young germ-free mice transplanted with gut microbiota of old mice [6], we first detected neurogenesis in each of the four treatment groups by detecting the number of DCX^+ (a marker for migrating neuronal cells) hippocampal neurons in the DG of mice. As shown in Fig. 9, MPTP treatment markedly increased DCX^+ neurons in the DG of PD mice (YM + MPTP and AM + MPTP group), which might be a compensative mechanism for MPTP-induced cell death, as reported before [40]. Notably, AM + MPTP mice had more DCX^+ neurons in the DG than YM + MPTP mice (Fig. 9A–B). We further investigated adult neurogenesis by detecting the number of Ki67-positive ($Ki67^+$, a marker for cell proliferation) hippocampal cells in the DG. Consistently, AM + MPTP mice exhibited more $Ki67^+$ cells in the DG than YM + MPTP mice (Fig. 9C–D). In addition, there was a significant increase in the expression of the cellular stemness marker (*CD133*) in the hippocampus of AM + MPTP mice compared to YM + MPTP mice (Fig. 9E). All these results collectively indicate that FMT from aged donors enhances MPTP-induced neurogenesis in the hippocampus.

Discussion

We demonstrate a distinct difference of gut microbiota between young and aged mice. For example, there is decrease in SCFA-producing bacteria, including *Ruminococcaceae UCG-014* [28–30] and *Eubacterium xylanophilum* group [31], as well as an increase of beneficial genera *Lactobacillus* in aged mice than those in young mice. *Ruminococcaceae UCG-014* are reported to be related with the combination of quercetin and resveratrol in relieving high-fat diet-induced obesity [41] and have been associated with ameliorating dextran sodium sulfate-induced colitis [42]. *Lactobacillus* probiotics alleviate neurodegeneration in a Drosophila melanogaster AD model [43] and exhibit therapeutic potential for improving memory deficits in aged SAMP8 mice [44]. Studies have increasingly suggested that the effects of age-related microbiota on a young host include changes in host immunity, neurogenesis and cognition [6, 20, 21, 45]. We have found that gut microbiota modulation by fecal microbiota transplantation could affect both motor symptoms and neurotransmitter loss in MPTP-induced PD mice [35]. Considering the important role of gut microbiota in PD, age-related gut microbiota may have an impact on

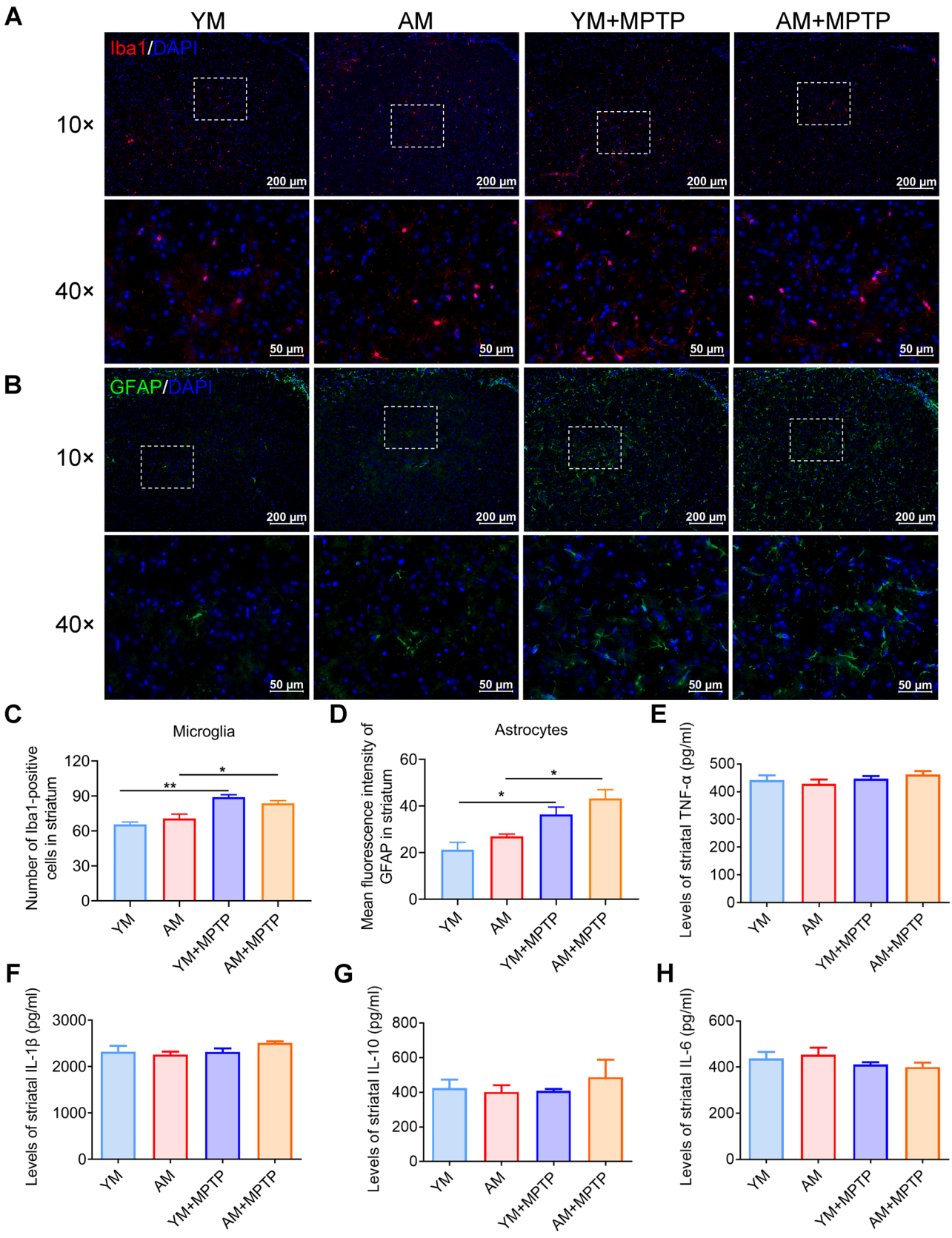
A
YM
AM
YM+MPTP
AM+MPTP
Iba1/DAPI
10×
40×
200 μm
50 μm
B
GFAP/DAPI
C
Microglia
Number of Iba1-positive cells in striatum
D
Astrocytes
Mean fluorescence intensity of GFAP in striatum
E
Levels of striatal TNF-α (pg/ml)
F
Levels of striatal IL-1β (pg/ml)
G
Levels of striatal IL-10 (pg/ml)
H
Levels of striatal IL-6 (pg/ml)

◂**Fig. 7** Effects of FMT from young and aged mice on neuroinflammation. **A** Immunostaining of Iba1 for microglia in the striatum. **B** Immunostaining of GFAP for astrocytes in the striatum. **C** Quantitative analysis of the number of Iba1-positive microglia in each group. **D** Quantitative analysis of the mean fluorescence intensity of GFAP in astrocytes in each group. N = 3 in each group. Scale bars in images with 40 × are 50 μm, and 10 × magnification are 200 μm. ELISA analysis of striatal **E** TNF-α, **F** IL-1β, **G** IL-10 and **H** IL-6 expression. N = 5 in each group. *: $P < 0.05$ and **: $P < 0.01$

the occurrence of PD. Hence, the purpose of this study was to uncover the influence of transplanting the gut microbiota from an aging host on PD mice. Although transplantation of gut microbiota from aged mice could not upregulate the striatal DA content or TH protein, it significantly suppressed the loss of dopaminergic neurons in the SNpc of PD mice. We also found that transplantation of gut microbiota from aged mice could significantly resist MPTP-induced motor

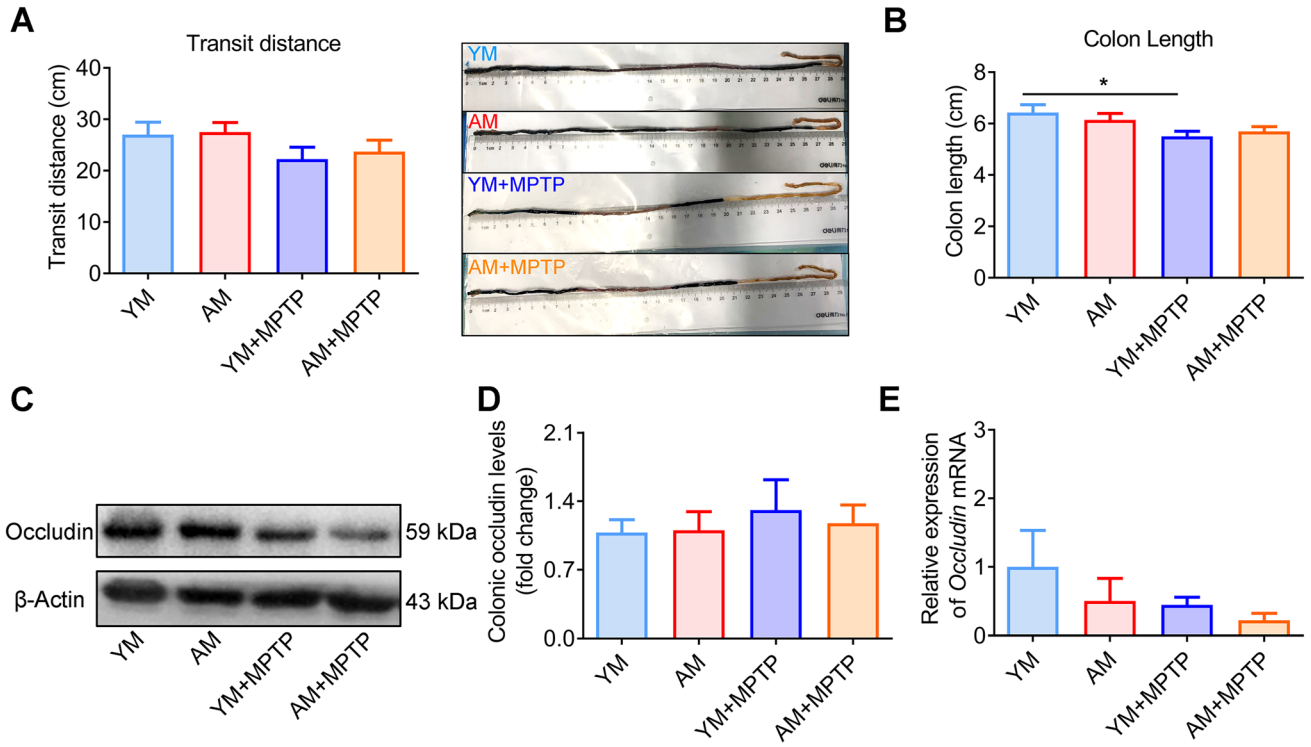

F

Cytokines (colon qPCR)	YM	AM	YM+MPTP	AM+MPTP
	Mean±S.E.M	Mean±S.E.M	Mean±S.E.M	Mean±S.E.M
Tnf-α	1.00±0.52	0.97±0.36	1.02±0.81	1.10±0.93
Il-1β	1.00±0.70	0.45±0.54	0.46±0.27	1.26±0.69
Il-6	1.00±1.02	0.95±1.10	0.15±0.10	0.14±0.05
iNos	1.00±0.72	0.85±0.19	0.79±0.14	0.68±0.12
Il-18	1.00±0.41	0.42±0.43	1.16±0.69	1.31±0.65
Il-10	1.00±0.45	1.46±0.45	0.71±0.51	0.83±0.29
Il-4	1.00±0.34	1.14±0.31	0.56±0.37	0.63±0.30
Tgf-β	1.00±0.40	0.85±0.30	1.25±0.47	1.07±0.36

Fig. 8 Effects of FMT from young and aged mice on gastrointestinal physiology and inflammation. **A** Left: intestinal transit distance; Right: representative image of intestines containing Evans blue dye. **B** Colon length, n = 7 for YM and AM groups, and n = 9 for YM + MPTP and AM + MPTP groups (exception: n = 6 in the YM group in the intestinal transit test). **C** Western blotting for occludin protein expression detection. **D** Quantification of occludin expression in the colon. **E** *Occludin* mRNA in the colon, determined by qRT-PCR. **F** Relative mRNA expression of various inflammatory cytokines in the colon. For WB: n = 7 in each group. For qRT-PCR: n = 6 ~ 7 in each group. *: $P < 0.05$

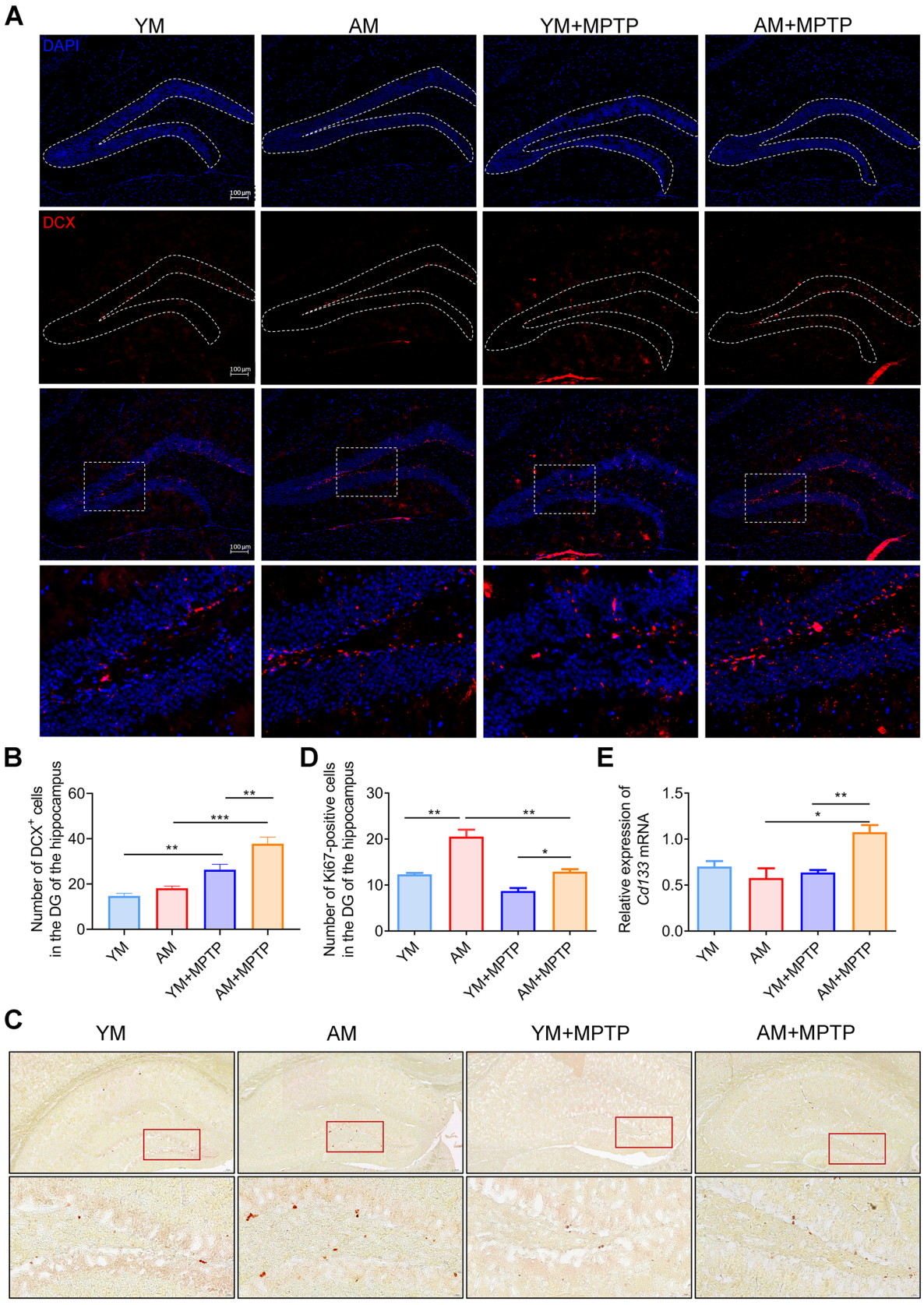
A
YM
AM
YM+MPTP
AM+MPTP
DAPI
DCX
100 μm
B
Number of DCX+ cells in the DG of the hippocampus
60
40
20
0
**
***
**
YM
AM
YM+MPTP
AM+MPTP
D
Number of Ki67-positive cells in the DG of the hippocampus
30
20
10
0
**
**
*
YM
AM
YM+MPTP
AM+MPTP
E
Relative expression of Cd133 mRNA
1.5
1.0
0.5
0.0
**
*
YM
AM
YM+MPTP
AM+MPTP
C
YM
AM
YM+MPTP
AM+MPTP

◂**Fig. 9** Effects of FMT from young and aged mice on hippocampal neurogenesis. **A** Representative images showing DCX staining of neurons (red) and DAPI (blue) in the DG. Scale bars is 100 μm. **B** Quantification of DCX^+ neurons in the DG. **C** Representative images showing Ki67 staining. The enlarged image boxed in red is shown underneath. **D** Quantification of $Ki67^+$ cells in the DG, n = 5 in each group. Scale bar: 100 μm (up) and 20 μm (down). **E** Relative expression of hippocampal *Cd133* mRNA, n = 6 ~ 9 in each group. *: $P < 0.05$; **: $P < 0.01$ and ***: $P < 0.001$

dysfunction (indicated by the shorter descent time in the pole test and an extended running duration in the rotarod test), decline of striatal 5-HT content and higher metabolic rate of DA (indicated by the decreased HVA/DA ratio). Our findings imply that transplanting gut microbiota from an aged host may have a neuroprotective effect in PD.

Changes in gut microbiota composition are strongly associated with age-related neurodegenerative diseases, including PD and AD [46, 47]. Given the fact that distinct differences in fecal microbiota exist between young and aged hosts, we further explore the underlying mechanism of the effect of aged microbiota on the occurrence of PD by high-throughput sequencing. No significant difference was observed in α-diversity, suggesting few structural differences among the four groups. However, β-diversity, as indicated by the clear separation, shows a remarkable change in the composition of microbiota between YM + MPTP and AM + MPTP groups. Additionally, the *Akkermansia* and *Candidatus Saccharimonas* abundance were decreased in the YM + MPTP group and dramatically increased in AM + MPTP mice, indicating their potential role in the protective effects of aged microbiota on PD. *Akkermansia*, a potential next-generation probiotic, is associated with the host mucus turnover, which improves gut barrier function, and is also decreased in a PD mouse model [48]. According to previous studies, *Akkermansia* could effectively improve symptoms in several diseases, such as ulcerative colitis [49], obesity [50] and amyotrophic lateral sclerosis [51], by protecting gut barrier function and reducing levels of inflammatory cytokines (TNF-α, IL-1β, IL-6) in the colon. Luo et al. found that the relative abundance of *Candidatus Saccharimonas* is reduced in db/db mice, and this change is reversed in db/db mice treated with inulin-type fructans [52]. Although a study has shown that there is a greater abundance of *Rikenellaceae RC9 gut* group at the genus level in fecal samples from PD patients [53], we detected no significant change in PD mice in this study, but AM + MPTP mice exhibited a higher abundance of *Rikenellaceae RC9 gut* group. The same trend was observed in sulfate-reducing bacteria *Desulfovibrio* in AM + MPTP mice.

Thus, how does FMT from aged mice contribute to the resistance to MPTP in mice? Among the potential changes associated with aging microbiota, SCFAs in the gut may be one of major mediators [19, 20]. It is well known that SCFAs play a crucial role in regulating central nervous system processes (such as neurotransmitter levels, brain glia activation, as well as expression of genes related to inflammatory response, intestinal barrier, and oxidative stress). Further experiments by GC–MS revealed that transplantation of the gut microbiota from aged donor mice decreased the abnormal elevation of fecal SCFAs in adult recipient mice. As reported before, Lee and colleagues found that aging of host decreased the concentration of primary SCFAs in fecal samples of young (2–3 months) and aged (18–20 months) mice [19]. This is consistent with results from Fig. 1G showing decreases in SCFA-producing bacteria in aged mice. The abnormal elevation of SCFAs in YM + MPTP mice is also in line with our previous study showing that sodium butyrate exacerbated PD through aggravating neuroinflammation and colonic inflammation of PD mice [54]. FMT from aged donors could promote the restoration of normal fecal SCFA levels in mice. Furthermore, we performed correlation analyses and found that the fecal SCFAs were positively correlated with motor dysfunction and DA metabolism, and negatively correlated with striatal 5-HT content.

It is well accepted that neuroinflammation, characterized by activation of microglia and astrocytes, is responsible for the loss of dopaminergic neurons in the SNpc, and the reduction of striatal dopamine content of PD patients [55, 56]. Neuroinflammatory processes also play a crucial role in aging, and there has been increasing attention paid to the role of microglia and astrocytes [57]. Erny et al. found that activation of microglia is under constant regulation by the gut microbiome [58]. A sharp increase was observed in the number of microglia and astrocytes in the striatum of YM + MPTP mice and AM + MPTP mice. Unexpectedly, the number of microglia and astrocytes in AM + MPTP mice did not change significantly compared with that in the YM + MPTP group. To further confirm whether the neuroprotective effect mediated by FMT with aged microbiota is related to the alleviation of neuroinflammation, we measured the content of striatal TNF-α, IL-1β, IL-10 and IL-6 by ELISA. There were no significant changes in these cytokines among the four groups, nor were there statically significant differences in gut permeability or gut inflammation. This partly suggests that the neuroprotective effect of aged microbiota transplantation acts in a neuroinflammation-independent manner.

Aging is usually associated with reduced neurogenesis in the adult brain [59]. Impaired adult neurogenesis [60, 61] and decreased expression of neurogenic markers are also present in PD [62]. Moreover, the number of DCX-positive neurons in the DG is also reduced in PD model animals [63, 64]. All these suggest that impaired hippocampal neurogenesis may be one of the causes of PD. Recently, Kundu et al. found that transplantation of old donor gut microbiota into

young germ-free recipient mice could enhance neurogenesis in the hippocampus of the brain and promote intestinal growth [6]. Inspired by their work, we focused on the neurogenesis in both young and aged FMT recipients in our study. Surprisingly, our data are consistent with the notion that neurogenesis is increased in PD animal models, as reported by Ryu's group [40]. This might be due to a compensative mechanism induced by MPTP-induced cell death. One novel finding of the current study is that transplantation of gut microbiota of aged mice enhances hippocampal neurogenesis after MPTP treatment. This unexpected finding emphasizes the current limited understanding of alterations of the gut microbiota, as well as the complex interplay between the host and the microbiota during aging. The present study implies that fecal microbiota transplantation protects against motor dysfunction, dopaminergic neuron loss, neurotransmitter decline and DA metabolism of MPTP-treated mice by inhibiting abnormal elevation of SCFA production and increasing endogenous adult neurogenesis in the DG.

Yet, several limitations exist in the current study, including the inherent limitations of FMT into antibiotic-treated, pseudo-germ-free mice, as antibiotic treatment can only maximize the removal of gut microbiota, which cannot be completely equivalent to germ-free mice. In this regard, future investigations based on germ-free mice will be needed to elucidate the effect of aged microbiota on PD pathology. Another limitation of our research is the lack of dynamic detection of gut microbiota changes during the experiment.

Conclusions

In summary, our findings, including recovery of motor function, alleviating loss of dopaminergic neurons in the SNpc, increasing striatal 5-HT content, inhibiting DA metabolism, restoring fecal SCFA levels and promoting neurogenesis in the DG of the hippocampus of PD mice, suggest that aged microbiota could effectively aid in resistance to the pathological features of PD in an inflammation-independent and neurogenesis-dependent manner. This research provides fundamental evidence that the gut microbiota should be considered as a potential therapeutic target for treating aspects of aging-associated neurodegenerative disease. Future studies should further elucidate the direct mechanistic underpinnings of how specific gut microbes, or specific metabolites, drive these changes in rejuvenating functions of the CNS.

Acknowledgements This study was supported by National Natural Science Foundation of China (81771384, 81801276, 82171429), Postgraduate Research and Practice Innovation Program of Jiangsu Province (KYCX19 1893), Public Health Research Center at Jiangnan University (JUPH201801), Youth Foundation of Basic Research Program of Jiangnan University in 2021 (JUSRP121063). We are grateful to Dr. Stanley Li Lin for his critical revision on the manuscript, both on language and science.

Authors' Contributions The experiment design and management: Chen-Meng Qiao and Yan-Qin Shen; Animal experiment operation: Chen-Meng Qiao, Yu-Zhou, Wei Quan, Gu-Yu Niu and Xiao-Yu Ma; Tissue collection: Chen-Meng Qiao, Yu-Zhou, Wei Quan, Gu-Yu Niu, Yun Shi, Li-Ping Zhao, Xiao-Yu Ma, Hui Hong and Jian Wu; HPLC/16S rRNA: Chen-Meng Qiao, Yu Zhou and Wei Quan; Quantitative real-time PCR analysis: Yu Zhou and Wei Quan; IF/IHC and image analysis: Yu Zhou, Wei Quan, Chen-Meng Qiao, Xiao-Yu Ma and Wei-Jiang Zhao; Western bolt: Yu Zhou and Wei Quan; Nissl staining: Chen-Meng Qiao, Wei Quan and Xiao-Yu Ma; Statistical analysis: Chen-Meng Qiao and Yu Zhou; Writing and revising of manuscript: Chen-Meng Qiao and Yan-Qin Shen.

Data Availability The data that support the findings of this study are available from the corresponding author upon reasonable request.

Declarations

Conflict of Interests The authors declare that they have no competing interests.

References

1. Ang QY, Alexander M, Newman JC, et al. Ketogenic diets alter the gut microbiome resulting in decreased intestinal Th17 cells. Cell. 2020;181:1263-1275.e1216. https://doi.org/10.1016/j.cell.2020.04.027.
2. Desai MS, Seekatz AM, Koropatkin NM, et al. A dietary fiber-deprived gut microbiota degrades the colonic mucus barrier and enhances pathogen susceptibility. Cell. 2016;167:1339-1353.e1321. https://doi.org/10.1016/j.cell.2016.10.043.
3. Rooks MG, Garrett WS. Gut microbiota, metabolites and host immunity. Nat Rev Immunol. 2016;16:341–52. https://doi.org/10.1038/nri.2016.42.
4. Sharon G, Sampson TR, Geschwind DH, Mazmanian SK. The central nervous system and the gut microbiome. Cell. 2016;167:915–32. https://doi.org/10.1016/j.cell.2016.10.027.
5. Braniste V, Al-Asmakh M, Kowal C, et al. The gut microbiota influences blood-brain barrier permeability in mice. Sci Transl Med. 2014;6:263ra158. https://doi.org/10.1126/scitranslmed.3009759.
6. Kundu P, Lee HU, Garcia-Perez I, et al. Neurogenesis and prolongevity signaling in young germ-free mice transplanted with the gut microbiota of old mice. Sci Transl Med. 2019;11:eaau4760. https://doi.org/10.1126/scitranslmed.aau4760.
7. Mosher KI, Wyss-Coray T. Go with your gut: microbiota meet microglia. Nat Neurosci. 2015;18:930–1. https://doi.org/10.1038/nn.4051.
8. Sampson TR, Debelius JW, Thron T, et al. Gut microbiota regulate motor deficits and neuroinflammation in a model of Parkinson's disease. Cell. 2016;167:1469-1480.e1412. https://doi.org/10.1016/j.cell.2016.11.018.
9. Sun MF, Shen YQ. Dysbiosis of gut microbiota and microbial metabolites in Parkinson's Disease. Ageing Res Rev. 2018;45:53–61. https://doi.org/10.1016/j.arr.2018.04.004.
10. Scheperjans F, Aho V, Pereira PA, et al. Gut microbiota are related to Parkinson's disease and clinical phenotype. Mov Disord. 2015;30:350–8. https://doi.org/10.1002/mds.26069.

11. Cryan JF, O'Riordan KJ, Sandhu K, Peterson V, Dinan TG. The gut microbiome in neurological disorders. Lancet Neurol. 2020;19:179–94. https://doi.org/10.1016/S1474-4422(19)30356-4.
12. Cersosimo MG, Raina GB, Pecci C, et al. Gastrointestinal manifestations in Parkinson's disease: prevalence and occurrence before motor symptoms. J Neurol. 2013;260:1332–8. https://doi.org/10.1007/s00415-012-6801-2.
13. Pont-Sunyer C, Hotter A, Gaig C, et al. The onset of nonmotor symptoms in Parkinson's disease (the ONSET PD study). Mov Disord. 2015;30:229–37. https://doi.org/10.1002/mds.26077.
14. Unger MM, Spiegel J, Dillmann KU, et al. Short chain fatty acids and gut microbiota differ between patients with Parkinson's disease and age-matched controls. Parkinsonism Relat Disord. 2016;32:66–72. https://doi.org/10.1016/j.parkreldis.2016.08.019.
15. Vascellari S, Melis M, Palmas V, et al. Clinical phenotypes of Parkinson's disease associate with distinct gut microbiota and metabolome enterotypes. Biomolecules. 2021;11:144. https://doi.org/10.3390/biom11020144.
16. Keshavarzian A, Green SJ, Engen PA, et al. Colonic bacterial composition in Parkinson's disease. Mov Disord. 2015;30:1351–60. https://doi.org/10.1002/mds.26307.
17. Torres ERS, Akinyeke T, Stagaman K, et al. Effects of Subchronic MPTP exposure on behavioral and cognitive performance and the microbiome of wild-type and mGlu8 knockout female and male mice. Front Behav Neurosci. 2018;12:140. https://doi.org/10.3389/fnbeh.2018.00140.
18. Fransen F, van Beek AA, Borghuis T, et al. Aged gut microbiota contributes to systemical inflammaging after transfer to germ-free mice. Front Immunol. 2017;8:1385. https://doi.org/10.3389/fimmu.2017.01385.
19. Lee J, d'Aigle J, Atadja L, et al. Gut microbiota-derived short-chain fatty acids promote poststroke recovery in aged mice. Circ Res. 2020;127:453–65. https://doi.org/10.1161/Circresaha.119.316448.
20. Spychala MS, Venna VR, Jandzinski M, et al. Age-related changes in the gut microbiota influence systemic inflammation and stroke outcome. Ann Neurol. 2018;84:23–36. https://doi.org/10.1002/ana.25250.
21. D'Amato A, Di Cesare ML, Lucarini E, et al. Faecal microbiota transplant from aged donor mice affects spatial learning and memory via modulating hippocampal synaptic plasticity- and neurotransmission-related proteins in young recipients. Microbiome. 2020;8:140. https://doi.org/10.1186/s40168-020-00914-w.
22. Cao Q, Qin L, Huang F, et al. Amentoflavone protects dopaminergic neurons in MPTP-induced Parkinson's disease model mice through PI3K/Akt and ERK signaling pathways. Toxicol Appl Pharmacol. 2017;319:80–90. https://doi.org/10.1016/j.taap.2017.01.019.
23. Perez-Pardo P, Dodiya HB, Engen PA, et al. Role of TLR4 in the gut-brain axis in Parkinson's disease: a translational study from men to mice. Gut. 2019;68:829–43. https://doi.org/10.1136/gutjnl-2018-316844.
24. Zhou ZL, Jia XB, Sun MF, et al. Neuroprotection of fasting mimicking diet on MPTP-induced Parkinson's disease mice via gut microbiota and mtabolites. Neurotherapeutics. 2019;16:741–60. https://doi.org/10.1007/s13311-019-00719-2.
25. Garcia-Villalba R, Gimenez-Bastida JA, Garcia-Conesa MT, Tomas-Barberan FA, Carlos Espin J, Larrosa M. Alternative method for gas chromatography-mass spectrometry analysis of short-chain fatty acids in faecal samples. J Sep Sci. 2012;35:1906–13. https://doi.org/10.1002/jssc.201101121.
26. Zhao L, Zhang F, Ding X, et al. Gut bacteria selectively promoted by dietary fibers alleviate type 2 diabetes. Science. 2018;359:1151–6. https://doi.org/10.1126/science.aao5774.
27. Nagpal R, Mainali R, Ahmadi S, et al. Gut microbiome and aging: Physiological and mechanistic insights. Nutr Healthy Aging. 2018;4:267–85. https://doi.org/10.3233/NHA-170030.
28. Liu YQ, Hu XY, Zheng W, et al. Action mechanism of hypoglycemic principle 9-(R)-HODE isolated from cortex lycii based on a metabolomics approach. Front Pharmacol. 2022. https://doi.org/10.3389/fphar.2022.1011608.
29. Tian BM, Zhao JH, Zhang M, et al. Lycium ruthenicum anthocyanins attenuate high-fat diet-induced colonic barrier dysfunction and inflammation in mice by modulating the gut microbiota. Mol Nutr Food Res. 2021. https://doi.org/10.1002/mnfr.202000745.
30. Lopez-Montoya P, Cerqueda-Garcia D, Rodriguez-Flores M, et al. Association of gut microbiota with atherogenic dyslipidemia, and its impact on serum lipid levels after bariatric surgery. Nutrients. 2022. https://doi.org/10.3390/nu14173545.
31. Zhuge A, Li S, Yuan Y, Li B, Li L. The synergy of dietary supplements Lactobacillus salivarius LI01 and Bifidobacterium longum TC01 in alleviating liver failure in rats treated with D-galactosamine. Food Funct. 2021;12:10239–52. https://doi.org/10.1039/d1fo01807h.
32. Amabebe E, Robert FO, Agbalalah T, Orubu ESF. Microbial dysbiosis-induced obesity: role of gut microbiota in homoeostasis of energy metabolism. Br J Nutr. 2020;123:1127–37. https://doi.org/10.1017/S0007114520000380.
33. O'Mahony SM, Clarke G, Borre YE, Dinan TG, Cryan JF. Serotonin, tryptophan metabolism and the brain-gut-microbiome axis. Behav Brain Res. 2015;277:32–48. https://doi.org/10.1016/j.bbr.2014.07.027.
34. Jang JH, Yeom MJ, Ahn S, et al. Acupuncture inhibits neuroinflammation and gut microbial dysbiosis in a mouse model of Parkinson's disease. Brain Behav Immun. 2020;89:641–55. https://doi.org/10.1016/j.bbi.2020.08.015.
35. Sun MF, Zhu YL, Zhou ZL, et al. Neuroprotective effects of fecal microbiota transplantation on MPTP-induced Parkinson's disease mice: Gut microbiota, glial reaction and TLR4/TNF-alpha signaling pathway. Brain Behav Immun. 2018;70:48–60. https://doi.org/10.1016/j.bbi.2018.02.005.
36. Singh R, Chandrashekharappa S, Bodduluri SR, et al. Enhancement of the gut barrier integrity by a microbial metabolite through the Nrf2 pathway. Nat Commun. 2019;10:89. https://doi.org/10.1038/s41467-018-07859-7.
37. Kim N, Jeon SH, Ju IG, et al. Transplantation of gut microbiota derived from Alzheimer's disease mouse model impairs memory function and neurogenesis in C57BL/6 mice. Brain Behav Immun. 2021;98:357–65. https://doi.org/10.1016/j.bbi.2021.09.002.
38. Wei GZ, Martin KA, Xing PY, et al. Tryptophan-metabolizing gut microbes regulate adult neurogenesis via the aryl hydrocarbon receptor. Proc Natl Acad Sci USA. 2021;118:e2021091118. https://doi.org/10.1073/pnas.2021091118.
39. Ma XY, Xiao WC, Li H, et al. Metformin restores hippocampal neurogenesis and learning and memory via regulating gut microbiota in the obese mouse model. Brain Behav Immun. 2021;95:68–83. https://doi.org/10.1016/j.bbi.2021.02.011.
40. Ryu S, Jeon H, Koo S, Kim S. Korean red ginseng enhances neurogenesis in the subventricular zone of 1-methyl-4-phenyl-1,2,3,6-tetrahydropyridine-treated mice. Front Aging Neuroscience. 2018;10:355. https://doi.org/10.3389/fnagi.2018.00355.
41. Zhao L, Zhang Q, Ma W, Tian F, Shen H, Zhou M. A combination of quercetin and resveratrol reduces obesity in high-fat diet-fed rats by modulation of gut microbiota. Food Funct. 2017;8:4644–56. https://doi.org/10.1039/c7fo01383c.
42. Hu L, Jin L, Xia D, et al. Nitrate ameliorates dextran sodium sulfate-induced colitis by regulating the homeostasis of the intestinal microbiota. Free Radical Biol Med. 2020;152:609–21. https://doi.org/10.1016/j.freeradbiomed.2019.12.002.
43. Tan FHP, Liu G, Lau SA, et al. Lactobacillus probiotics improved the gut microbiota profile of a Drosophila melanogaster Alzheimer's disease model and alleviated neurodegeneration in the eye. Benef Microbes. 2020;11:79–89. https://doi.org/10.3920/BM2019.0086.
44. Yang X, Yu D, Xue L, Li H, Du J. Probiotics modulate the microbiota-gut-brain axis and improve memory deficits in aged SAMP8 mice. Acta Pharm Sin B. 2020;10:475–87. https://doi.org/10.1016/j.apsb.2019.07.001.

45. Li Y, Ning L, Yin Y, et al. Age-related shifts in gut microbiota contribute to cognitive decline in aged rats. Aging (Albany NY). 2020;12:7801–17. https://doi.org/10.18632/aging.103093.
46. Cuervo-Zanatta D, Garcia-Mena J, Perez-Cruz C. Gut microbiota alterations and cognitive impairment are sexually dissociated in a transgenic mice model of Alzheimer's disease. J Alzheimers Dis. 2021;82:S195–214. https://doi.org/10.3233/JAD-201367.
47. Bhattarai Y, Si J, Pu M, et al. Role of gut microbiota in regulating gastrointestinal dysfunction and motor symptoms in a mouse model of Parkinson's disease. Gut Microbes. 2021;13:1866974. https://doi.org/10.1080/19490976.2020.1866974.
48. Zhou XT, Lu JC, Wei KH, et al. Neuroprotective effect of ceftriaxone on MPTP-induced Parkinson's disease mouse model by regulating inflammation and intestinal microbiota. Oxid Med Cell Longev. 2021;2021:9424582. https://doi.org/10.1155/2021/9424582.
49. Bian XY, Wu WR, Yang LY, et al. Administration of Akkermansia muciniphila ameliorates dextran sulfate sodium-induced ulcerative colitis in mice. Front Microbiol. 2019;10:2259. https://doi.org/10.3389/fmicb.2019.02259.
50. Yang YJ, Zhong ZQ, Wang BJ, et al. Early-life high-fat diet-induced obesity programs hippocampal development and cognitive functions via regulation of gut commensal Akkermansia muciniphila. Neuropsychopharmacology. 2019;44:2054–64. https://doi.org/10.1038/s41386-019-0437-1.
51. Blacher E, Bashiardes S, Shapiro H, et al. Potential roles of gut microbiome and metabolites in modulating ALS in mice. Nature. 2019;572:474–80. https://doi.org/10.1038/s41586-019-1443-5.
52. Luo LM, Luo JL, Cai YT, et al. Inulin-type fructans change the gut microbiota and prevent the development of diabetic nephropathy. Pharmacol Res. 2022;183:106367. https://doi.org/10.1016/j.phrs.2022.106367.
53. Yan ZZ, Yang F, Cao JW, et al. Alterations of gut microbiota and metabolome with Parkinson's disease. Microb Pathog. 2021;160:105187. https://doi.org/10.1016/j.micpath.2021.105187.
54. Qiao CM, Sun MF, Jia XB, et al. Sodium butyrate exacerbates Parkinson's disease by aggravating neuroinflammation and colonic inflammation in MPTP-induced mice model. Neurochem Res. 2020;45:2128–42. https://doi.org/10.1007/s11064-020-03074-3.
55. Bagetta V, Ghiglieri V, Sgobio C, Calabresi P, Picconi B. Synaptic dysfunction in Parkinson's disease. Biochem Soc Trans. 2010;38:493–7. https://doi.org/10.1042/BST0380493.
56. Calabresi P, Di Filippo M, Ghiglieri V, Tambasco N, Picconi B. Levodopa-induced dyskinesias in patients with Parkinson's disease: filling the bench-to-bedside gap. Lancet Neurol. 2010;9:1106–17. https://doi.org/10.1016/S1474-4422(10)70218-0.
57. Jyothi HJ, Vidyadhara DJ, Mahadevan A, et al. Aging causes morphological alterations in astrocytes and microglia in human substantia nigra pars compacta. Neurobiol Aging. 2015;36:3321–33. https://doi.org/10.1016/j.neurobiolaging.2015.08.024.
58. Erny D, Hrabe de Angelis AL, Jaitin D, et al. Host microbiota constantly control maturation and function of microglia in the CNS. Nat Neurosci. 2015;18:965–77. https://doi.org/10.1038/nn.4030.
59. Apple DM, Solano-Fonseca R, Kokovay E. Neurogenesis in the aging brain. Biochem Pharmacol. 2017;141:77–85. https://doi.org/10.1016/j.bcp.2017.06.116.
60. Marchetti B, Tirolo C, L'Episcopo F, et al. Parkinson's disease, aging and adult neurogenesis: Wnt/β-catenin signalling as the key to unlock the mystery of endogenous brain repair. Aging Cell. 2020;19:e13101. https://doi.org/10.1111/acel.13101.
61. Winner B, Winkler J. Adult neurogenesis in neurodegenerative diseases. Cold Spring Harb Perspect Biol. 2015;7:021287. https://doi.org/10.1101/cshperspect.a021287.
62. Hoglinger GU, Rizk P, Muriel MP, et al. Dopamine depletion impairs precursor cell proliferation in Parkinson disease. Nat Neurosci. 2004;7:726–35. https://doi.org/10.1038/nn1265.
63. Singh S, Mishra A, Mishra SK, Shukla S. ALCAR promote adult hippocampal neurogenesis by regulating cell-survival and cell death-related signals in rat model of Parkinson's disease like-phenotypes. Neurochem Int. 2017;108:388–96. https://doi.org/10.1016/j.neuint.2017.05.017.
64. Zhang T, Hong J, Di T, Chen L. MPTP impairs dopamine D1 receptor-mediated survival of newborn neurons in ventral hippocampus to cause depressive-like behaviors in adult mice. Front Mol Neurosci. 2016;9:101. https://doi.org/10.3389/fnmol.2016.00101.